



HAL
open science

Mitigating the open vessel artefact in centrifuge-based measurement of embolism resistance

Rosa Ana Lopez Rodriguez, Markus Nolf, Remko A. Duursma, Eric Badel, Richard J. Flavel, Hervé Cochard, Brendan Choat

► **To cite this version:**

Rosa Ana Lopez Rodriguez, Markus Nolf, Remko A. Duursma, Eric Badel, Richard J. Flavel, et al.. Mitigating the open vessel artefact in centrifuge-based measurement of embolism resistance. *Tree Physiology*, 2019, 39 (1), pp.143-155. 10.1093/treephys/tpy083 . hal-01854603

HAL Id: hal-01854603

<https://hal.science/hal-01854603v1>

Submitted on 6 Aug 2018

HAL is a multi-disciplinary open access archive for the deposit and dissemination of scientific research documents, whether they are published or not. The documents may come from teaching and research institutions in France or abroad, or from public or private research centers.

L'archive ouverte pluridisciplinaire **HAL**, est destinée au dépôt et à la diffusion de documents scientifiques de niveau recherche, publiés ou non, émanant des établissements d'enseignement et de recherche français ou étrangers, des laboratoires publics ou privés.

Mitigating the open vessel artefact in centrifuge based measurement of embolism resistance

Journal:	<i>Tree Physiology</i>
Manuscript ID	TP-2018-172.R1
Manuscript Type:	Methods paper
Date Submitted by the Author:	n/a
Complete List of Authors:	Rosana, Lopez; Universidad Politecnica de Madrid, Sistemas y Recursos Naturales; Université Clermont Auvergne, INRA, PIAF Nolf, Markus ; western sydney university, Hawkesbury Institute for the Environment Duursma, Remko; Western Sydney University Hawkesbury Institute for the Environment Badel, Eric; Université Clermont Auvergne, INRA, PIAF Flavel, Richard; University of New England, School of Environmental and Rural Science Cochard, Hervé; Université Clermont Auvergne, INRA, PIAF Choat, Brendan; Western Sydney University Hawkesbury Institute for the Environment
Keywords:	Xylem Embolism, Drought Resistance, vulnerability to cavitation, cavitron, centrifuge technique, x-ray micro CT


 SCHOLARONE™
 Manuscripts

1 **Title:** Mitigating the open vessel artefact in centrifuge based measurement of embolism resistance

2 **Running head:** Mitigating artefacts in vulnerability curves

3

4

5 Rosana López^{1,2}, Markus Nolf³, Remko A Duursma³, Eric Badel¹, Richard J Flavel⁴, Hervé Cochard¹,

6 Brendan Choat³

7

8 1- Université Clermont Auvergne, INRA, PIAF, Clermont-Ferrand, France.

9 2- Sistemas y Recursos Naturales, Universidad Politécnica de Madrid, Madrid, Spain.

10 3- Hawkesbury Institute for the Environment, Western Sydney University, Richmond, NSW, Australia.

11 4- School of Environmental and Rural Science, University of New England, Armidale, NSW, Australia.

12

13 **Corresponding author details:**

14 Dr. Rosana López

15 e-mail: rosana.lopez@upm.es

16 phone: +34 655868659

17 Address: ETSI Montes, Forestal y del Medio Natural. C/ José Antonio Novais, 10. 28040 Madrid

18

19

1
2
3 20 **Abstract** (300 words max)
4

5
6 21 Centrifuge-based techniques to assess xylem vulnerability to embolism are increasingly being used,
7
8 22 although we are yet to reach a consensus on the nature and extent of artefactual embolism
9
10 23 observed in some angiosperm species. In particular, there is disagreement over whether these
11
12 24 artefacts influence both the spin (Cavitron) and static versions of the centrifuge technique equally.
13

14
15 25 We tested two methods for inducing embolism: bench dehydration and centrifugation. We used
16
17 26 three methods to measure the resulting loss of conductivity: gravimetric flow measured in bench-
18
19 27 dehydrated and centrifuged samples (static centrifuge), in situ flow measured under tension during
20
21 28 spinning in the centrifuge (Cavitron), and direct imaging using X-ray microCT observations in stems
22
23 29 of two species of *Hakea* that differ in vessel length.
24

25
26 30 Both centrifuge techniques were prone to artefactual embolism in samples with maximum vessel
27
28 31 length longer, or similar, to the centrifuge rotor diameter. Observations with microCT indicated that
29
30 32 this artefactual embolism occurred in the outer most portions of samples. The artefact was largely
31
32 33 eliminated if flow was measured in an excised central part of the segment in the static centrifuge or
33
34 34 starting measurements with the Cavitron at pressures lower than the threshold of embolism
35
36 35 formation in open vessels. The simulations of loss of conductivity in centrifuged samples with a new
37
38 36 model, CAVITOPEN, confirmed that the impact of open vessels on the vulnerability to embolism
39
40 37 curve was higher when vessels were long, samples short and when embolism is formed in open
41
42 38 vessels at less negative pressures. This model also offers a robust and quantitative tool to test and
43
44 39 correct for artefactual embolism at low xylem tensions.
45
46

47
48 40 **Keywords**
49

50
51 41 Vulnerability to embolism, xylem embolism, drought, centrifuge technique, Cavitron, X-Ray microCT,
52
53 42 CAVITOPEN.
54

55
56 43
57
58
59
60

44 Introduction

45 Xylem water transport is dependent upon water held in a metastable state of water; evaporation of
46 water from the leaf cell walls generates tension, which is transmitted through the water column to
47 the roots. Water under tension is prone to cavitation, i.e. the abrupt transition from a metastable
48 liquid to a gas, resulting in the formation of gas emboli that block the xylem conduits and impairs
49 water transport (Tyree and Sperry 1988). As tension in the xylem sap increases, for example during
50 drought, so does the probability of embolism formation. During severe or prolonged droughts,
51 hydraulic failure can result in the complete loss of hydraulic conductance in the xylem and
52 subsequent canopy dieback, or whole plant death (Brodribb and Cochard 2009; Nardini et al. 2013;
53 Rodríguez-Calcerrada et al. 2017; Urli et al. 2013; Venturas et al. 2016). Hydraulic failure is now
54 considered a principal cause of drought-induced plant mortality and forest die off (Choat et al. 2012;
55 Sala et al. 2010). The projected rise in global mean temperature and frequency of extreme climate
56 events over the next century will impact forest ecosystems and shift species distribution ranges. In
57 this sense, resistance to embolism has emerged as a crucial parameter to understanding species
58 ecology, differences in water use strategies, and for predicting future mortality events (Brodribb
59 2017).

60 Xylem resistance to embolism is usually characterized with a vulnerability curve, showing the
61 decrease in hydraulic conductivity as a function of the xylem tension. Since the publication of the
62 first vulnerability curves for woody plants were published in 1985 (Sperry 1985) and 1986 (Tyree and
63 Dixon 1986), a number of techniques that allow for more rapid measurement of vulnerability have
64 been introduced (see Cochard et al. (2013) for a detailed review). However, although the time
65 required for construction of a vulnerability curve has been dramatically reduced, recent work
66 suggests that some of these methods are prone to experimental artefact (Choat et al. 2010; Cochard
67 et al. 2010; Sperry et al. 2012; Torres-Ruiz et al. 2014). This has led to re-examination of
68 methodology used to measure vulnerability to embolism (Jansen et al. 2015).

1
2
3 69 The most straightforward technique for inducing embolism is bench dehydration, wherein whole
4
5 70 plants or long branches are gradually dehydrated to various xylem tensions and hydraulic
6
7 71 conductivity of excised segments is measured gravimetrically before and after removing air from
8
9 72 embolised conduits (Sperry and Tyree 1988; Tyree and Zimmermann 2002). Bench dehydration relies
10
11 73 on natural desiccation of plant tissues and is therefore considered as the best reference method
12
13 74 with which to validate other techniques (Cochard et al. 2013; Ennajeh et al. 2011; Sperry et al. 2012).
14
15 75 This method is not completely free of artefacts and issues associated with disequilibrium in water
16
17 76 potential within a stem, blockage of flow by resin/mucilage (Cobb et al. 2007), and excision of
18
19 77 samples under tension can all alter the vulnerability curve significantly (Wheeler et al., 2013).
20
21 78 Although most of these issues can be minimised by adoption of suitable protocols (eg. Torres-Ruiz et
22
23 79 al., 2015), the bench dehydration technique requires several days and a substantial amount of plant
24
25 80 material to obtain a vulnerability curve for one species. As such, Holbrook et al. (1995) and Pockman
26
27 81 et al. (1995) proposed the use of a centrifugal force to create a defined negative pressure in the
28
29 82 xylem sap of excised plant stems, allowing for rapid and consistent generation of vulnerability
30
31 83 curves. Pockman et al. (1995) constructed vulnerability curves for several species by comparing the
32
33 84 hydraulic conductivity before and after spinning branches with their ends exposed to air, removing
34
35 85 segments at both ends before measuring conductivity in the remaining, middle section of the
36
37 86 sample. Alder et al. (1997) modified this technique with a centrifuge rotor designed to keep the
38
39 87 segment ends immersed in water during spinning, allowing the conductivity of a single segment to
40
41 88 be remeasured at different tensions to create an entire vulnerability curve for a single sample. This
42
43 89 important innovation allowed repeated measurements to be made on the same plant material,
44
45 90 reducing the number of samples required for construction of a curve and strengthening the results
46
47 91 statistically. Finally, Cochard (2002), Cochard et al. (2005) and Li et al. (2008) further modified the
48
49 92 centrifuge method and designed new rotors which allowed measuring the conductivity of the
50
51 93 segment while it is spinning and under tension. This further increased the efficiency of measurement
52
53 94 and allowed for flow measurements to be made under tension.
54
55
56
57
58
59
60

1
2
3 95 Although centrifuge based techniques induce embolism by increasing tension in sample xylem, the
4
5 96 patterns of embolism spread through the sample may differ from a naturally dehydrated sample (Cai
6
7 97 et al. 2010). The tension profile in the centrifuged segment is highest in the axis of rotation (i.e. in
8
9 98 the middle section of the segment) and declines towards the segment ends (Cochard et al. 2005),
10
11 99 while during natural dehydration the tension profile across the segment is expected to remain
12
13 100 approximately constant (Cai et al. 2010). Nevertheless, the vulnerability curves generated by
14
15 101 centrifugation agree well with the bench-top method in conifers and short-vesseled angiosperm
16
17 102 species (Alder et al. 1997; Cochard et al. 2005; Cochard et al. 2010; Li et al. 2008). In contrast,
18
19 103 inconsistent results have been obtained for species with long vessels, specifically those in which a
20
21 104 significant number of vessels in the sample are longer than the centrifuge rotor (Choat et al. 2010;
22
23 105 Jacobsen and Pratt 2012; Sperry et al. 2012; Torres-Ruiz et al. 2014).

24
25
26 106 Since 2005 the number of vulnerability curves constructed by centrifugation has increased
27
28 107 exponentially (see Fig. 3 in Cochard et al. (2013)). Accordingly, considerable effort has been devoted
29
30 108 to testing and validation of centrifuge techniques, whether measuring the flow gravimetrically after
31
32 109 spinning (static centrifuge method), or while centrifuging (Cavitron method). However, we are yet to
33
34 110 reach a consensus on the nature and extent of artefactual embolism observed with centrifuge
35
36 111 techniques. In particular, there is disagreement over whether these artefacts influence both spin
37
38 112 (Cavitron rotor) and static versions of the centrifuge technique equally (Hacke et al. 2015; Sperry et
39
40 113 al. 2012). In recent years, the application of x-ray computed microtomography (microCT) to the
41
42 114 study of plant hydraulics has emerged as a potentially powerful tool to validate hydraulic
43
44 115 techniques. In addition to providing a non-invasive assay of xylem function, it allows for analyses of
45
46 116 spatial and temporal patterns of embolism formation (Brodersen et al. 2013; Choat et al. 2016;
47
48 117 Dalla-Salda et al. 2014; Torres-Ruiz et al. 2016).

49
50
51
52
53 118 In this study we evaluated the performance of both centrifuge techniques against bench
54
55 119 dehydration in order to examine possible discrepancies associated with each technique. First, we

1
2
3 120 tested two methods for inducing embolism: bench dehydration and centrifugation. We then tested
4
5 121 three ways of measuring the resulting loss of conductivity: gravimetric flow measured in bench-
6
7 122 dehydrated and centrifuged samples (static centrifuge), *in situ* flow measured under tension during
8
9 123 spinning in the centrifuge (Cavitron), and direct imaging using X-ray microCT observation. All
10
11 124 experiments were carried out with two species of the genus *Hakea* that differ in vessel length. *H.*
12
13 125 *dactyloides* is a short vesseled species with maximum vessel length shorter than 14 cm, whereas *H.*
14
15 126 *leucoptera* has longer vessels and maximum vessel length is ca. 25 cm. Additionally, we compared
16
17 127 results obtained using two rotor diameters (14 and 27 cm) to assess the effect of sample length, and
18
19 128 measured hydraulic flow both in the whole, spun segments and excised middle sections. Spatial
20
21 129 patterns of embolism within samples were visualized with X-ray microCT after centrifugation in
22
23 130 order to provide further insight into potential discrepancies. Finally, a new model, CAVITOPEN was
24
25 131 developed to simulate the effect of vessel and sample lengths on centrifuge estimates of embolism
26
27 132 resistance. We hypothesized that i) both centrifuge techniques, the static centrifuge and the
28
29 133 cavitron, are prone to similar artefacts when constructing vulnerability curves of long-vesseled
30
31 134 species; ii) the shape of the vulnerability curve of centrifuged samples will depend on the amount of
32
33 135 cut open vessels; iii) image techniques and standard flow measurements will produce similar
34
35 136 vulnerability curves.
36
37
38

39 137 **Material and methods**

40 138 *Plant Material*

41
42
43
44
45 139 Experiments were carried out on branch material of two diffuse-porous species of the same genus
46
47 140 exhibiting different vessel lengths, *Hakea dactyloides* (Gaertn.) Cav. and *Hakea leucoptera* R. Br.
48
49 141 Branches were sampled from natural populations of *H. dactyloides* at Mount Banks (33° 34' 46" S,
50
51 142 150° 21' 56" E; NSW, Australia) and *H. leucoptera* at Binya State Forest (34° 11' 16" S, 146° 16' 13"
52
53 143 E; NSW, Australia) from May to September 2016 (late autumn-winter in the South Hemisphere). Sun
54
55 144 exposed branches of 1.5-2.0 m length were collected in the field in the early morning and
56
57
58
59
60

1
2
3 145 immediately placed in black plastic bags with moistened paper towels to prevent transpiration with
4
5 146 their cut ends covered with Parafilm. In the laboratory they were kept at 4 °C until measured.
6
7

8 147 *Midday xylem water potential in the field and Native embolism*
9

10
11 148 Midday xylem water potential was measured in the field in November 2015, February 2016 and June
12
13 149 2016. Two leaves of five plants per species were covered with aluminium foil and sealed with a
14
15 150 plastic bag 1 hour before excision and measurement with a pressure chamber (PMS Instrument Co.,
16
17 151 Albany, OR, USA).
18

19
20 152 Native embolism was determined in current-year, one-year and two-year old segments of 5
21
22 153 branches per species to ensure that the effects of previous natural water stress were minimised.
23

24 154 Note that segments containing 1-year and 2-year-old growth were necessary to fit in the 27 cm rotor
25

26 155 of the centrifuge. Measuring native embolism we also wanted to control for sample collection date
27
28 156 because branches were cut at different times during late autumn-winter 2016 to avoid long storage.
29

30 157 Branch proximal end was cut underwater to release tension for 30 min (Torres-Ruiz et al. 2015;
31
32 158 Wheeler et al. 2013) and then the branch was progressively recut under water to segments 50 mm
33

34 159 long. Note that at least twice the maximum vessel length was removed from the cut end after
35
36 160 tension relaxation. Thereafter, the edges of these segments were trimmed using a razor blade. Initial
37

38 161 conductivity (K_h) was measured in 50 mm long segments with filtered, degassed 2 mmol KCl solution
39
40 162 at low pressure (≤ 4 kPa) with a liquid flowmeter (LiquiFlow L13-AAD-11-K-10S; Bronkhorst High-
41
42 163 Tech B.V., Ruurlo, the Netherlands). The segments were then flushed with the same solution at a
43

44
45 164 minimum of 0.20 MPa for 15 min to remove embolism and subsequently determine maximum
46
47 165 hydraulic conductivity (K_{max}). The native percentage loss of conductivity (PLC) was calculated for
48

49 166 each segment as:
50
51

52 167 $PLC = 100 \times (1 - K_h / K_{max})$ (equation 1)
53
54
55
56
57
58
59
60

1
2
3 168 Specific hydraulic conductivity (K_S) was calculated dividing K_{max} by the xylem cross-sectional area
4
5 169 (average distal and proximal xylem area measured with a calliper).
6

7
8 170 *Maximum vessel length and vessel length distribution*
9

10
11 171 Ten branches per species were sampled from the same plants as used for hydraulic measurements
12
13 172 to determine maximum vessel length with the air perfusion technique (Ewers and Fisher 1989). Once
14
15 173 in the lab, 60 cm long segments were flushed for 1 h with degassed, filtered 2 mmol KCl solution at
16
17 174 0.18-0.20 MPa to remove any embolism. Then each segment was infiltrated with compressed air at
18
19 175 0.05 MPa at its distal end with an aquarium air pump while the basal end was repeatedly shortened
20
21 176 by 2 cm under water until air bubbles emerged. The remaining sample length was assumed as
22
23 177 maximum vessel length.
24

25
26 178 An estimate of the amount of vessels longer than the centrifuge rotor diameter and longer than half
27
28 179 the rotor diameter (open to centre vessels) was assessed in four branches of *H. dactyloides* and five
29
30 180 branches of *H. leucoptera* by measuring the decrease in PLC after air injection (Cochard et al. 1994;
31
32 181 Torres-Ruiz et al. 2014). Briefly, 35 cm long segments were flushed as described above to remove
33
34 182 embolism. Then, tubing was attached to the distal end of these segments and compressed air was
35
36 183 injected into the samples at 0.1 MPa for 10 min using a pressure chamber. This pressure was
37
38 184 sufficient to empty the open vessels but not high enough to move water through wet pit membranes
39
40 185 between adjacent vessels (Ewers and Fisher, 1989). PLC was determined in 3 cm long segments
41
42 186 across the sample as described for native embolism. At the injection point, PLC is close to 100%
43
44 187 because all the vessels are air filled and progressively decrease to 0 for a length longer than the
45
46 188 longest vessel in the sample. The PLC at each distance from the injection point corresponds to the
47
48 189 percentage of contribution to flow from vessels longer than this distance. If all the vessels were of
49
50 190 equal diameter, this percentage would correspond to the number of vessels longer than the distance
51
52 191 from the injection point. In this case of the two *Hakea* species used are diffuse porous and vessel
53
54 192 diameters within the same sample did not vary greatly. Thus the curves in Fig. 1 represent a proxy of
55
56
57
58
59
60

1
2
3 193 vessel distribution of the two species, although not as accurate as anatomy, and allow to estimate
4
5 194 the amount of open vessels from a certain cut point.

6
7
8 195 *Bench dehydration technique*

9
10 196 Branches were dehydrated gradually in the laboratory at ca. 23 °C. Xylem water potential (Ψ_x) was
11
12 197 measured with a pressure chamber (PMS Instrument Co., Albany, OR, USA) in bagged leaves
13
14 198 (wrapped with aluminium foil and a plastic bag at least 1 h before sampling). When the target Ψ_x to
15
16 199 construct the VC was reached, branches were sealed into a plastic bag with moistened paper towels
17
18 200 for 1 h to equilibrate Ψ_x . Water potential was measured again in two bagged leaves of the same
19
20 201 branchlet to confirm homogeneous Ψ_x in the sample. The Ψ_x of the sample was considered
21
22 202 equilibrated if the difference between the three Ψ_x (one measured before sealing the branch and
23
24 203 two measured after equilibration) was not higher than 0.1 MPa. Afterwards tension was released for
25
26 204 30 minutes by cutting the branch proximal end under water and PLC was determined in one-year-old
27
28 205 segments as for native embolism. Vulnerability curves were generated by plotting PLC against Ψ_x .
29
30 206 For *H. leucoptera* 7 branches were dehydrated and 4 different branchlets per branch were measured
31
32 207 at different Ψ_x to construct the vulnerability curve and for *H. dactyloides* we used 12 branches and
33
34 208 two branchlets per branch. All branchlets were far apart (at least four branch orders) and after
35
36 209 collection the cutting surface was covered with parafilm to avoid air entry in the rest of the sample.
37
38
39
40

41 210 *Centrifuge techniques*

42
43
44 211 We compared two centrifuge techniques: i) the static centrifuge method described by Alder et al.
45
46 212 (1997) and ii) the *in situ* flow technique (Cavitron (Cochard 2002; Cochard et al. 2005)). In the static
47
48 213 centrifuge two different sizes of custom-built rotors, 14 cm and 27 cm, were used to test the effect
49
50 214 of segment length and fraction of open vessels. All hydraulic conductivity measurements were
51
52 215 performed using filtered, degassed 2 mmol KCl solution and a flow meter (see Native embolism
53
54 216 section).

1
2
3 217 Static centrifuge measurements were carried out on 20 branches per species. Branches were
4
5 218 trimmed under water and both ends were shaved to a final length of 14 or 27 cm. The initial
6
7 219 hydraulic conductivity was measured as described above (see Native embolism section) with a
8
9 220 pressure head of 7.5 kPa. Subsequently, 14-cm long branches were spun in the centrifuge (Sorvall RC
10
11 221 5C Plus) for 5 minutes at increasing pressure steps. Foam pads saturated with the solution used for
12
13 222 measurements were placed in the reservoirs of the rotor to maintain sample ends in contact with
14
15 223 the solution even when the rotor was stopped (Tobin et al. 2013). After each step, samples were
16
17 224 removed and K_h was measured on the whole segment as described for native embolism. In the
18
19 225 27cm-long branches we modified the single spin method (Hacke et al. 2015) so that two
20
21 226 measurements were made in each centrifuged segment. The initial K_h was measured before spinning
22
23 227 in the 27-cm long sample. After spinning, K_h was measured on the whole segment and the first PLC
24
25 228 was calculated. Subsequently, a 4 cm-long segment was cut from the middle section and its K_h was
26
27 229 measured. The second PLC was determined in this 4 cm-long segment after flushing to obtained the
28
29 230 maximum K_h (K_{max}) as described for native embolism.

30
31
32
33 231 *In situ* flow centrifuge measurements (Cavitron technique) were carried out on six branches per
34
35 232 species using a modified bench top centrifuge (H2100R, Cence Xiangyi, Hunan, China). For the static
36
37 233 centrifuge, samples were trimmed under water to a length of 27 cm to fit in the rotor. Initial
38
39 234 conductivity, K_i , was determined at a xylem pressure of -0.5 MPa in *H. dactyloides* and 1.5 MPa in *H.*
40
41 235 *leucoptera*. The xylem pressure was then lowered stepwise by increasing the rotational velocity, and
42
43 236 K_h was again determined while the sample was spinning. The PLC at each pressure step was
44
45 237 quantified as

46
47
48 238
$$\text{PLC} = 100 \times (1 - K_h / K_i).$$
 (equation 2)
49

50
51 239 *X-ray microCT imaging*
52
53
54
55
56
57
58
59
60

1
2
3 240 A subset of branches of *H. leucoptera* was transported to the University of New England in Armidale
4
5 241 (NSW, Australia). They were gradually dehydrated to five different xylem water potentials ranging
6
7 242 from -4.8 MPa to -9 MPa as for the bench dehydration method. After measuring Ψ_x , tension was
8
9 243 relaxed by cutting the proximal end of the branch under water leaving it submerged for 30 minutes.
10
11 244 Then the branch was sequentially cut back under water and finally 10-mm-long segments were
12
13 245 excised under water from current-year shoots, wrapped in Parafilm, inserted into a plexiglass tube
14
15 246 and then placed in an X-ray microtomography system (GE-Phoenix V|tome|xs, GE Sensing &
16
17 247 Inspection Technologies, Wunstorf, Germany) to visualize embolized vessels. Another subset of
18
19 248 branches of *H. leucoptera* was centrifuged to five (-5, -6, -7, -8, -9 MPa) and three (-5, -6, -7 MPa)
20
21 249 different water potentials in the static centrifuge using 27 cm and 14 cm long segments,
22
23 250 respectively. They were immediately submerged in liquid paraffin wax and preserved at 4 °C for
24
25 251 three days until measured in the same facility (Cochard et al. 2015). Seven branches of *H. dactyloides*
26
27 252 were also centrifuged at four (-3, -4, -5, -6 MPa) and three (-3, -4, -5 MPa) water potentials with the
28
29 253 27 and 14 cm rotors, respectively, following the same protocol. One branch of *H. leucoptera* was
30
31 254 prepared as the centrifuged samples but was not spun in the centrifuge to detect any possible
32
33 255 artefact due to sample preparation. All samples were scanned at the middle of the sample.
34
35 256 Additionally, in three 27 cm long samples we scanned at 6 cm and 12 cm from the axis of rotation to
36
37 257 examine embolism profiles across a sample.
38
39
40
41 258 X-ray scan settings were 90 kV and 170 mA, and 1800 projections, 600 ms each, were acquired
42
43 259 during the 360° rotation of the sample. The resultant images covered the whole cross section of the
44
45 260 sample in 8.7 mm length with a spatial resolution of 8.7 μm per voxel. At the end of the scan, the
46
47 261 sample was cut back to 30 mm length, injected with air at >1 MPa pressure and rescanned at the
48
49 262 same location as before to visualize all empty vessels in the fully embolized cross section. After
50
51 263 three-dimensional reconstruction with Phoenix datos|x2 Reconstruction Version 2.2.1-RTM (GE
52
53 264 Sensing & Inspection Technologies, Wunstorf, Germany), volumes were imported into ImageJ 1.49k
54
55 265 (Schneider et al. 2012). A median Z projection of c. 100 μm along the sample axis was extracted from
56
57
58
59
60

1
2
3 266 the middle of the scan volumes following the protocol in Nolf et al. (2017). PLC of each sample was
4
5 267 estimated calculating the theoretical hydraulic conductance based on the conduit dimensions of
6
7 268 embolized and functional vessels (Choat et al. 2016). To measure conduit dimensions, a radial sector
8
9 269 of the transverse section was selected in the same microCT scan and all their embolized vessels were
10
11 270 measured manually. The image of this sector was then binarized so the dimensions of the selected
12
13 271 embolized vessels matched with the manually drawn vessels. This threshold value was then used for
14
15 272 binarizing the image of the whole cross section and all the embolized vessels were measured using
16
17 273 the Analyse Particles function in Image J. Theoretical specific hydraulic conductivity (K_{sth}) was
18
19 274 calculated as:

$$23 \quad K_{sth} = \frac{\sum \left(\frac{D^4 \pi}{128 \eta} \cdot \frac{\Delta p}{\Delta x} \right)}{A} \quad \text{(equation 3)}$$

25
26 276

27
28 277 Where D is the equivalent circular vessel diameter based on vessel area, η viscosity of water, $\Delta p/\Delta x$
29
30 278 pressure gradient per xylem length, A xylem cross-sectional area.

31
32 279

33
34 280 The current theoretical specific hydraulic conductivity (K_{sth}) for each sample was calculated by
35
36 281 subtracting the summed specific hydraulic conductivity of embolized vessels from the $K_{sth(max)}$ of that
37
38 282 sample, calculated as the K_{sth} of the sample after air injection. The pressure gradient used for
39
40 283 calculations of K_{sth} was similar to the pressure gradient used in the hydraulic measurements, 0.06
41
42 284 MPa m⁻¹.

43 44 285 *Vulnerability curve fitting and statistical analysis*

45
46
47 286 Vulnerability curves were fitted using a Weibull function (Ogle et al. 2009) in R 3.2.0 (R Core Team,
48
49 287 2015) using the fitplc package (Duursma and Choat 2017). Confidence intervals of P_{12} , P_{50} and P_{88} (Ψ_x
50
51 288 at 12, 50 and 88 % loss of conductivity, respectively) and the slope of the curve at 50% loss of
52
53 289 conductivity (S_{50}) were used to compare between methods. Confidence intervals (CI) for the bench

290 dehydration and the static centrifuge techniques were obtained using bootstrap resampling (999
 291 replicates). Methods were considered to be statistically different if the 95% CIs did not overlap.

292 Differences in native embolism and specific initial conductivity between sampling dates were tested
 293 with a one-way ANOVA. Means were compared using a Tukey test at 95% confidence. Vulnerability
 294 curve parameters across methods were compared at the Ψ_x corresponding with three levels of loss
 295 of conductivity: 12%, 50% and 88% (P_{12} , P_{50} and P_{88} , respectively) and the slope of the VC at 50% loss
 296 of conductivity (S_{50}).

297 *CAVITOPEN- simulation of the effect of open vessels in a centrifuged sample*

298 To disentangle the effects of centrifugation on 'true' vessel embolism at the centre of the samples,
 299 where more vessels are closed at both ends and tension is maximum, from draining of open vessels
 300 at both sample ends a new model, CAVITOPEN, was developed. In a centrifuged sample, the
 301 variation of xylem pressure (P) with distance from the axis of rotation (r) is given by the following
 302 equation (Alder et al. 1997):

$$303 \quad dP/dr = \rho\omega^2 r \quad \text{(equation 4)}$$

304 where ρ is the density of water, and ω the angular velocity.

305 Integrating this equation from R (distance from the axis of rotation to the water reservoir) we can
 306 obtain the pressure at r (P_r):

$$307 \quad P_r = 0.5 \rho\omega^2 (R^2 - r^2) \quad \text{(equation 5)}$$

308 The effect of vessel length on 'true' vessel embolism in a spun sample has already been modelled by
 309 Cochard et al (2005). Briefly, if the vessels are infinitely long, the VC obtained by centrifugation
 310 should yield the correct P_{50} value. When the vessels are infinitely short the P_{50} value is
 311 underestimated due to the variation of xylem pressure inside the spun sample (eq. 4) and the
 312 consequent gradient of embolism along the sample: xylem pressure is minimum in the middle of the

1
2
3 313 sample and null at the extremities (eq. 5). Since the loss of conductivity is measured on the whole
4
5 314 sample, an underestimation of the degree of embolism in the middle of the sample is predicted. This
6
7 315 effect of vessel length was further tested with the CAVITOPEN model and found marginal, i.e. the
8
9 316 shift in the VC was negligible, compared to the draining effect. For sake of simplicity, this effect was
10
11 317 no longer considered in the simulations. To simulate the draining effect at both sample ends, we first
12
13 318 hypothesized that vessel ends follow a logarithmic distribution following the vessel length
14
15 319 probability density function proposed by Cohen et al. (2003) and assuming vessel ends uniformly
16
17 320 distributed across the length of the sample:

20 321
$$N_x = N_0 \cdot \exp(-x/L_{max})$$
 (equation 6)

22
23 322 where N_x is the number of open vessels at the distance x from sample ends, N_0 the total number of
24
25 323 vessels and L_{max} the maximum vessel length.

26
27
28 324 The second assumption of the model is that open vessels drain when the minimum pressure in the
29
30 325 vessel exceeds a threshold value P_{open} . Because of the quadratic distribution of the pressure in the
31
32 326 sample, vessels having their end wall located closer to the sample ends, i. e. further from the centre
33
34 327 of rotation, will drain at a higher rotational velocity.

35
36
37 328 The branch segment was discretised in 0.1 mm thick sections arranged in serial. The xylem pressure
38
39 329 in the middle of the segment was set to a pressure varying from 0 to -12 MPa in 1 MPa steps. The
40
41 330 model then computes the pressure at steady state in each 0.1 mm section and determines the PLC
42
43 331 caused by 'true' embolism (non-open vessels) and by draining (open vessels). Finally, the PLC of the
44
45 332 whole segment is computed which enables the construction of the vulnerability curve. We tested
46
47 333 the model for different theoretical L_{max} values and the 4 rotors sizes used in our experiments. To
48
49 334 validate the model we used the values of PLC obtained for *H. leucoptera* in the static centrifuge with
50
51 335 the 27 cm rotor. The CAVITOPEN model was fit to the measurements using constrained numerical
52
53
54
55
56
57
58
59
60

336 optimization to estimate four parameters: P_{50} , S_{50} , L_{max} and P_{open} . All routines were implemented as
337 an R package (available from (Duursma 2017)).

338 Results

339 *Native embolism and minimum xylem water potential in the field.*

340 Midday xylem water potential decreased from -1.02 to -1.51 MPa in *H. dactyloides* and from -1.35 to
341 -2.62 MPa in *H. leucoptera* from November 2015 to February 2016. In June 2016, the water potential
342 was -1.16 MPa in *H. dactyloides* and -1.42 MPa in *H. leucoptera*. Native embolism remained low in
343 both species across the sampling dates. We measured higher PLC in two-year-old branch segments
344 (< 13 %) than in current year growth (< 2 %) in *H. leucoptera* whereas in *H. dactyloides* native
345 embolism was lower than 2% in all samples. Maximum xylem specific conductivity (K_{smax}) was $0.87 \pm$
346 $0.10 \text{ kg m}^{-1} \text{ s}^{-1} \text{ MPa}^{-1}$ in *H. leucoptera* and $1.29 \pm 0.09 \text{ kg m}^{-1} \text{ s}^{-1} \text{ MPa}^{-1}$ in *H. dactyloides* (mean \pm sd). No
347 significant differences in native PLC or K_s ($P > 0.05$; Table S1) were detected between sampling dates.

348 *Maximum vessel length and vessel length distribution*

349 Maximum vessel length as determined by air injection was 25 cm (standard deviation, sd = 5) in *H.*
350 *leucoptera* and 10 cm (sd = 3) in *H. dactyloides*. Air injected branches of *H. dactyloides* showed 17%
351 PLC at 7 cm from the injection point, 5% at 14 cm and less than 1% at 28 cm, whereas in *H.*
352 *leucoptera* the PLC was always higher, 50%, 25%, and 5% at 7, 14 and 28 cm respectively (Fig. 1).
353 Thus the number of open vessels at both ends when using the centrifuge technique differed
354 between species.

355 *Vulnerability curves*

356 Vulnerability curves (VCs) obtained with the bench dehydration technique were s-shaped for both
357 species, with significant embolism only occurring once a threshold water potential had been
358 reached. This threshold was more negative in *H. leucoptera* (-6.3 MPa) than in *H. dactyloides* (-3.8

1
2
3 359 MPa) (Fig. 2). VCs obtained with bench dehydration had the most negative P_{12} and the steepest
4
5 360 slopes of all methods (Table S2), meaning that embolism formation started at more negative Ψ_x and
6
7 361 conductivity was lost across a narrower range of Ψ_x compared with VCs generated by centrifugation.
8
9
10 362 When the centrifuge was used to induce embolism, results in the shorter-vesseled species, *H.*
11
12 363 *dactyloides*, were similar for the three techniques used to measure loss of conductivity, flowmeter,
13
14 364 Cavitron and microCT (average P_{50} with the 27 cm rotor in the static centrifuge and the Cavitron -4.8
15
16 365 MPa), and the CI at 95% overlapped with bench dehydration ($P_{50} = -5.0$ MPa). The VC generated with
17
18 366 the 14 cm rotor for *H. dactyloides* yielded slightly less negative values ($P_{50} = -4.3$ MPa; Table S2; Fig.
19
20 367 2). In contrast, VCs for *H. leucoptera* differed considerably depending on the method and the sample
21
22 368 length. Vulnerability parameters (P_{12} , P_{50} , P_{88}) obtained with the Cavitron (-5.0, -7.1 and -9.0 MPa,
23
24 369 respectively) matched more closely with the bench dehydration VC (-6.3, -7.4 and -8.2 MPa). For
25
26 370 samples spun in the static centrifuge, we found a significant effect both of the rotor size and the
27
28 371 segment used to measure flow (whole, spun segment or excised middle section in the 27 cm rotor)
29
30 372 on apparent vulnerability to embolism: segments measured across their entire length exhibited
31
32 373 higher vulnerability to embolism compared to the bench-dehydration VC as shown by P_{12} (-1.2 and -
33
34 374 2.6 MPa for 14 and 27 cm rotors, respectively) and P_{50} (-5.3 and -6.0 MPa, respectively), but seemed
35
36 375 less vulnerable towards the dry end of the curve (P_{88} of -14.2 and -10.4 MPa, respectively; Table S2).
37
38 376 Both VCs were almost linear when flow was measured across the whole segment with a shift
39
40 377 towards more vulnerable values with the 14 cm rotor, but became s-shaped when only the middle
41
42 378 section of the 27 cm segment was measured (Fig. 2). Removing the segment ends resulted in a
43
44 379 steeper slope and significantly more negative values of P_{12} and P_{50} . The Cavitron and the middle
45
46 380 segment techniques yielded similar results and agreed well with the dehydration technique in P_{50}
47
48 381 and P_{88} and with microCT image analysis (red triangles in Fig. 2).
49
50
51
52

53 382 *Patterns of embolism across a centrifuged sample*

1
2
3 383 Within 27-cm-length centrifuged samples of *H. leucoptera*, microCT scans revealed that embolism
4
5 384 levels were consistently at their highest near the sample ends (at 12 cm from the axis of rotation)
6
7 385 when spun at equivalents of -5, -7 and -9 MPa in the static centrifuge (Fig. 3). At -5 and -7 MPa loss
8
9 386 of conductivity decreased from the basal end to the centre, contradicting theoretical expectations.
10
11 387 This trend was observed even at Ψ_x inducing less than 40% PLC based on the bench dehydration VC
12
13 388 (Fig. 3). Only at -9 MPa, that is, below P_{88} on bench dehydration, did levels of embolism converge
14
15 389 along the length of the sample at 80-90%.

18 390 *Influence of open vessels in the VC of a centrifuged sample*

19
20
21 391 The simulations produced by the CAVITOPEN model confirmed that the shape of the VCs generated
22
23 392 by the centrifugation was largely dependent on vessel and sample lengths. As maximum vessel
24
25 393 length decreased, PLC of the whole sample decreased at a given Ψ_x , and the shape of the VC shifted
26
27 394 from exponential to sigmoidal (Fig. 4a). The same pattern was observed when the sample length
28
29 395 increased (Fig. 4b). For instance, with 14-cm-length centrifuged samples, P_{50} ranged from -0.6 MPa
30
31 396 to -7.7 MPa varying the maximum vessel length of the sample from 50 cm to 5 cm. Likewise, the P_{50}
32
33 397 of a centrifuged sample with maximum vessel length of 15 cm ranged from -2.1 MPa in the 14-cm
34
35 398 rotor to -7.7 MPa using a 40-cm rotor. Embolism of vessels open from the cut surface (Fig. S1)
36
37 399 influenced values of PLC at high negative pressures, even in short-veesled samples, resulting in
38
39 400 rapid loss of conductivity followed by a plateau. The more open vessels and the less negative the
40
41 401 threshold of embolism of open vessels (Fig. 4c), the higher is this plateau and stronger the impact on
42
43 402 the VC (Fig. 4). VCs can be corrected if the first inflection point of the curve is considered the starting
44
45 403 point for initial conductivity (K_i), i.e. 0% loss of conductivity. This is shown in Fig. 4d with actual
46
47 404 measurements of PLC obtained in 27-cm centrifuged samples of *H. leucoptera*. When the
48
49 405 CAVITOPEN model was fit (black circles and grey solid line, respectively) and we used the inflection
50
51 406 point as starting point for K_i , the corrected curve matched the reference VC obtained with bench
52
53 407 dehydration (Fig. 4d black solid line and orange dashed line, respectively). Alternatively, by fitting
54
55
56
57
58
59
60

1
2
3 408 the model using numerical optimization we estimated values of $P_{50} = -6.9$ MPa, $S_{50} = 49.7$, $L_{max} =$
4
5 409 15.21 and $P_{open} = -0.75$.

6 7 8 410 **Discussion**

9
10 411 We evaluated the reliability of two centrifuge based techniques commonly used to measure
11
12 412 vulnerability to embolism in angiosperm species and present a protocol that mitigates experimental
13
14 413 artefacts associated with open xylem vessels. Both the static centrifuge method and the *in-situ* flow
15
16 414 centrifuge method (Cavitron) were prone to artefactual embolism caused by open vessels, although
17
18 415 the errors were significantly greater in the static centrifuge method. In a species with maximum
19
20 416 vessel length longer or similar to the centrifuge rotor diameter, the static centrifuge significantly
21
22 417 overestimated xylem vulnerability to embolism if the whole spun segment was used to measure
23
24 418 flow. Observations with microCT indicated that artefactual embolism caused by centrifugation of
25
26 419 samples occurred in the outer most portions of samples. However, we demonstrated that
27
28 420 artefactual embolism was largely eliminated from static centrifuge if flow was measured in an
29
30 421 excised central part of the segment. This altered protocol yielded VCs similar to those obtained on
31
32 422 the same species with bench dehydration thus allowing these centrifuge techniques to accurately
33
34 423 measure vulnerability to embolism in longer vesseled species. We also present a new model
35
36 424 (CAVITOPEN) that simulates the impact of vessel draining at the cut end on the whole VC curve and
37
38 425 showed that errors were largely dependent on vessel length and rotor diameter. This model allows
39
40 426 researchers to quantitative test and avoid errors associated with the artefactual embolism. The
41
42 427 bench dehydration technique indicated that significant embolism was only initiated in both species
43
44 428 after water potential dropped below a threshold value, -3.8 MPa in *H. dactyloides* and -6.3 MPa in *H.*
45
46 429 *leucoptera*. PLC then increased rapidly and hydraulic conductivity was lost almost completely within
47
48 430 a span of 1 MPa (Fig. 2). These vulnerability curves have been classified as sigmoidal or s-shaped as
49
50 431 opposed to exponential or r-shaped curves, characterized by rapid conductivity losses as soon as the
51
52 432 water potential declines below zero (Cochard et al. 2013; Sperry et al. 2012). A third type of VC,

1
2
3 433 intermediate between these two, exhibits a linear response, and is mainly found in diffuse porous
4
5 434 species when using centrifugation to induce embolism (Cochard et al. 2013).
6

7
8 435 Our results showed that VCs obtained with the static centrifuge technique and the Cavitron are
9
10 436 similar to bench dehydration in a short-vesseled species, i.e. a species with no through vessels (open
11
12 437 at both ends) in the segment and with few vessels open from the cut surface to the middle of the
13
14 438 segment. All centrifuge generated VCs for *H. dactyloides* were sigmoidal and similar to bench
15
16 439 dehydration VCs, with a slight shift towards more vulnerable values when using the 14 cm rotor (Fig.
17
18 440 2, Table S2) as recently found by Pengxian et al. (2018) in *Acer mono* when comparing in the static
19
20 441 centrifuge the 14 cm and 27 cm rotors. VCs of other short vesseled angiosperms such as *Betula*
21
22 442 *pendula* (Cochard et al. 2010), *Fagus sylvatica* (Aranda et al. 2014), *Populus tremuloides* (Schreiber et
23
24 443 al. 2011) or *Acer negundo* (Christman et al. 2009) were also sigmoidal when the static centrifuge or
25
26 444 the Cavitron were used. In contrast, the VC shape obtained for *H. leucoptera* samples differed
27
28 445 significantly depending on methodology resulting in a shift of P_{50} of 2 MPa in samples from the same
29
30 446 population (Fig. 2, Table S2). This dramatic change was observed previously in peach (*Prunus persica*)
31
32 447 when the length of the centrifuged samples was varied in a Cavitron; shorter samples were more
33
34 448 vulnerable to embolism (P_{50} shifted from -4.5 to -1 MPa) and VCs became r-shaped (Cochard et al.
35
36 449 2010). However, when using the static centrifuge to measure the same population, Sperry et al.
37
38 450 (Sperry et al. 2012) found that VCs were linear and relatively insensitive to the number of open
39
40 451 vessels with P_{50} less negative than -2 MPa using 14 cm and 27 cm samples. This difference in
41
42 452 sensitivity to the proportion of open vessels in the centrifuged samples has led some to conclude
43
44 453 that the original centrifuge method and rotor design are not subject to the open vessel artefact
45
46 454 (Hacke et al. 2015; Sperry et al. 2012). However, Torres-Ruiz et al. (2017) demonstrated that if the
47
48 455 amount of open vessels is relatively high in both rotors, 14 and 27 cm, VCs could be equally biased
49
50 456 and would appear statistically indistinguishable.
51
52
53
54
55
56
57
58
59
60

1
2
3 457 Recent publications have addressed this controversy, showing that long-vesseled species such as
4
5 458 grape vine, oaks, robinia or olive, with a high proportion of open vessels, produce similarly biased
6
7 459 results with both the static centrifuge and the Cavitron when compared with reference curves
8
9 460 generated by dehydration or non-invasive imaging (Choat et al. 2016; Choat et al. 2010; Pengxian et
10
11 461 al. ; Torres-Ruiz et al. 2014). Li et al. (2008) and Pengxian et al. (2018) tested the two centrifuge
12
13 462 methods head to head and found close correspondence in VCs across species with different xylem
14
15 463 anatomy. An extended literature survey of methods to measure vulnerability to embolism showed
16
17 464 that when using the centrifuge, VCs were sigmoidal in conifers and in long vessel species
18
19 465 exponential, whereas in diffuse porous species VCs varied from sigmoidal to linear or exponential
20
21 466 (Cochard et al. 2013). Our measurements and simulations made with the CAVITOPEN model explain
22
23 467 the different shapes of VCs and some disagreements between the static centrifuge and the Cavitron.
24
25 468 In short-vesseled angiosperms, we have shown that VCs by centrifugation agreed with each other
26
27 469 and closely matched the curves based on bench dehydration and microCT (Choat et al. 2016;
28
29 470 Cochard et al. 2010). In angiosperms with a proportion of vessels open to the middle but not the
30
31 471 whole way through, the standard protocol in the static centrifuge produces linear VCs (Sperry et al.
32
33 472 2012). Here the initial conductivity is measured before spinning, thus if the native embolism is low,
34
35 473 all the vessels are conductive, regardless of their length. As soon as the sample is spun, the
36
37 474 conductivity would be artificially reduced relative to the native state in proportion to the amount of
38
39 475 vessels open to centre. Sample with open vessels thus become artificially vulnerable to embolism at
40
41 476 the beginning of the VC (i.e. at less negative water potentials). For *H. leucoptera*, this translated into
42
43 477 less negative values of P_{12} in all centrifuged samples compared with those measured with the bench
44
45 478 dehydration technique creating a linear response or a plateau at high water potentials. Higher
46
47 479 differences in P_{12} were observed in *H. leucoptera* than in *H. dactyloides* according with a higher
48
49 480 proportion of vessels open to centre in the former species (Fig. 1). In the Cavitron, the initial
50
51 481 measurement was made while spinning at low tension and many open to centre vessels would
52
53 482 already be embolised in the initial measurement of conductivity, resulting in a lower artefactual loss
54
55
56
57
58
59
60

1
2
3 483 of conductivity in the subsequent water potentials of the VC. This may bias the curves slightly
4
5 484 pushing them to more negative values but it did not appear to be significant effect here as the
6
7 485 Cavitron curves for *H. leucoptera* were similar to bench dehydration curves.
8
9

10 486 The simulations of PLC with the CAVITOPEN model confirmed that the impact of open vessels on the
11
12 487 VC was higher when vessels were long, samples short and when open vessels cavitated at less
13
14 488 negative pressures (Fig. 4). If the samples were much shorter than the maximum vessel length of the
15
16 489 branch (see the results in Fig. 4 for the 14 cm rotor with L_{max} 50cm), the resulting VC was exponential
17
18 490 (r-shaped), as observed in long-vesseled angiosperms, and shifted to more linear or s-shaped when
19
20 491 L_{max} was decreased or the sample length increased. One of the assumptions in the model is that
21
22 492 vessels open at the cut surface cavitate when they reach a threshold value; that is far less negative
23
24 493 than intact vessels whose two ends are included within the spun segment. This influences the shape
25
26 494 the VC at higher pressures creating a “bump” in the VC followed by a plateau. This effect can be
27
28 495 corrected to some extent if the first inflexion point of the VC is considered to be the 0% point for loss
29
30 496 of conductivity. In this case the initial conductivity (K_i) value is shifted to a lower value corresponding
31
32 497 to the hydraulic conductivity of the plateau (Fig. 4d). The estimated values of P_{50} and S_{50} when the
33
34 498 CAVITOPEN model was fit to actual measurements agreed quite well with those obtained with
35
36 499 reference techniques and confirmed that this model can be used to correct open vessel artefacts for
37
38 500 centrifuge based VCs. The estimated L_{max} was however significantly shorter than L_{max} measured with
39
40 501 the air injection technique. The air injection technique has shown to produce higher L_{max} than the
41
42 502 rubber injection method (Pan et al. 2015), thus our values could be overestimated. On the other
43
44 503 hand, the model assumed that vessel lengths in a sample follow the density function proposed by
45
46 504 Cohen et al. (2003) which can be sensitive to the clustering of vessel lengths (Cai and Tyree 2014). It
47
48 505 is clear that the actual distribution of vessel lengths, network topology and connectivity are crucial
49
50 506 for the sensitivity to an open vessel artefact.
51
52
53
54

55 **Origin of the open-vessel artefact**

56
57
58
59
60

1
2
3 508 The physical mechanisms underlying this open-vessel artefact are yet to be fully elucidated. Some
4
5 509 studies suggest that microbubbles and particles can act as nucleation sites when they flow through
6
7 510 the sample as it spins in the Cavitron, causing premature embolism (Cochard et al. 2010; Sperry et al.
8
9 511 2012; Wang et al. 2014). In the static centrifuge, bubbles might be drawn into vessels while starting
10
11 512 the spin or while mounting or dismounting the stems to measure flow (Wang et al. 2014). In both
12
13 513 centrifuge techniques bubbles in open vessels can move by buoyancy while spinning toward the
14
15 514 region of lowest pressure at the center of rotation (Rockwell et al., 2014). Draining from open
16
17 515 vessels as a consequence of artefactual embolism when the centrifuge starts spinning appears to be
18
19 516 a common phenomenon in both rotors. Our microCT images showed that after spinning in the
20
21 517 centrifuge, most of the vessels were empty near the ends even though tension ought to be zero
22
23 518 (Cochard et al. 2005). The use of water saturated foam pads to avoid desiccation did not prevent this
24
25 519 (Hacke et al. 2015; Tobin et al. 2013). We discarded the possibility that sample manipulation before
26
27 520 spinning or during wax embedding had triggered vessel draining because we scanned control
28
29 521 samples that were not spun. These samples showed no embolism (Fig. 3). Furthermore, patterns of
30
31 522 embolism did not follow theoretical expectations based on the distribution of tension within the
32
33 523 spun sample. The embolism levels decreased from the ends to the center in a fashion consistent
34
35 524 with the amount of vessels open to center, opposite to that expected from profile in tension and in
36
37 525 agreement with the assumption of the CAVITOPEN model than open vessels artificially cavitate
38
39 526 when they reach a threshold pressure that is much less negative than in intact vessels. This pattern
40
41 527 was observed at water potentials inducing less than 40% loss of conductivity based on the VC
42
43 528 obtained using the middle segment of the centrifuged sample (Fig. 3), even though the centre of the
44
45 529 sample experienced the highest tensions. Embolism levels converged within the sample at -9 MPa at
46
47 530 80-90%. These results confirm that centrifugation drains open vessels and only reliably measure the
48
49 531 vulnerability of intact xylem vessels within the sample (Fig. S1). This is consistent with observations
50
51 532 made previously by Cochard et al. (2010) using the Cavitron; they reported that embolism was
52
53 533 higher in the basal and upstream ends relative to the centre of samples from species with vessels
54
55
56
57
58
59
60

1
2
3 534 that are predominately at least half as long as the spun segment. Cai et al. (2010) and Pengxian et al.
4
5 535 (2018) also reported higher PLC values than predicted by theory at both ends after spinning samples
6
7 536 in a Cavitron. Given that our results were obtained with the static centrifuge it is clear that the
8
9 537 overestimation of vulnerability for open to centre vessels occurs in both versions of the centrifuge
10
11 538 technique.

12
13
14 539 The hydraulic continuity between vessels cut open at each end of the sample and vessels with their
15
16 540 terminal ends in this portion of the sample is probably re-established by refilling of vessels immersed
17
18 541 under water at both ends (Fig. 2 in Cochard et al. (2010)). This refilling would occur by capillarity
19
20 542 either while spinning in the Cavitron or while flow is measured gravimetrically (Fig. S2). Since the
21
22 543 middle of the centrifuged sample contains the majority of intact vessels, VCs constructed with the
23
24 544 static centrifuge technique of angiosperm species using only the central segment are more reliable
25
26 545 and in closer agreement with PLC generated by natural dehydration (Fig. 2). This modification is
27
28 546 technically easy to achieve and mitigates the open vessel artefact; however, it carries the
29
30 547 disadvantage that samples cannot be spun repeatedly to construct replicate curves for each sample
31
32 548 and thus more plant material is needed to construct each curve.

33 34 35 36 549 **Conclusion**

37
38
39 550 We confirmed the validity of vulnerability curves constructed with both centrifuge methods for short
40
41 551 conduit angiosperm species, those with most conduits shorter than half the length of the centrifuge
42
43 552 rotor. A new model, CAVITOPEN was developed to simulate the effect of vessel length, rotor size and
44
45 553 vulnerability of open vessels in loss of conductivity of centrifuged samples. In species with maximum
46
47 554 vessel length similar to the centrifuge rotor, we recommend constructing vulnerability curves with
48
49 555 the Cavitron or measuring flow exclusively in the central part of the spun segment when using the
50
51 556 static centrifuge. Alternatively, artefactual embolism at low xylem tensions can be corrected if the
52
53 557 first inflexion point of the VC is considered to be the starting point for K_{max} (0 % loss of conductivity)
54
55 558 or by fitting the CAVITOPEN model to the measurements to estimate P_{50} and S_{50} . When samples

1
2
3 559 contained a high proportion of open to centre vessels, the centrifuge technique is prone to error and
4
5 560 overestimates vulnerability to embolism. Determining the proportion of open to centre vessels or
6
7 561 performing the simple test recently proposed by Torres-Ruiz et al. (2017), which compares changes
8
9 562 in K_s before and after spinning in the centrifuge at low tensions, are highly advisable before using
10
11 563 any of the centrifuge techniques.

12
13
14 564 The shape of the vulnerability curves obtained with bench dehydration were always sigmoidal while
15
16 565 in centrifuged samples the shape was determined by the presence of open vessels. While previous
17
18 566 studies have demonstrated that species with the longest vessel classes (eg. lianas, ring porous trees)
19
20 567 open vessels tend to exhibit exponential curves when measured in the centrifuge. Here we showed
21
22 568 that VCs with a linear shape are symptomatic of species with intermediate vessel lengths in which a
23
24 569 higher proportion of vessels open to centre of the test segment. The occurrence of this incipient
25
26 570 open vessel artefact can be mitigated by measurement of the excised central portion of the
27
28 571 segment.

31 572 **Acknowledgments**

32
33
34 573 This research was supported by a Marie Curie Fellowship to R.L. (FP7PEOPLE-2013-IOF-624473) and
35
36 574 an ARC Future Fellowship to B.C. (FT130101115). We thank Dr. Javier Cano, Adrián Cano, Teresa
37
38 575 Rosas and Jennifer Peters for field assistance, Dr. Iain M Young for X-ray microCT advice and
39
40 576 comments on the manuscript, Gavin McKenzie for lab support and Dr. Stephanie Stuart for her ideas
41
42 577 and writing assistance. No conflict of interests declared.

43
44
45
46 578

579 **References**

- 580 Alder N, Pockman W, Sperry J, Nuismer S (1997) Use of centrifugal force in the study of xylem
581 cavitation. *Journal of Experimental Botany*. 48:665-674.
- 582 Aranda I, Cano FJ, Gascó A, Cochard H, Nardini A, Mancha JA, López R, Sánchez-Gómez D (2014)
583 Variation in photosynthetic performance and hydraulic architecture across European beech
584 (*Fagus sylvatica* L.) populations supports the case for local adaptation to water stress. *Tree*
585 *physiology*. 35:34-46.
- 586 Brodersen CR, McElrone AJ, Choat B, Lee EF, Shackel KA, Matthews MA (2013) In vivo visualizations
587 of drought-induced embolism spread in *Vitis vinifera*. *Plant Physiology*. 161:1820-9.
- 588 Brodrribb TJ (2017) Progressing from 'functional' to mechanistic traits. *New Phytologist*. 215:9-11.
- 589 Brodrribb TJ, Cochard H (2009) Hydraulic failure defines the recovery and point of death in water-
590 stressed conifers. *Plant Physiology*. 149:575-84.
- 591 Cai J, Hacke U, Zhang S, Tyree MT (2010) What happens when stems are embolized in a centrifuge?
592 Testing the cavitron theory. *Physiologia plantarum*. 140:311-320.
- 593 Cai J, Tyree MT (2014) Measuring vessel length in vascular plants: can we divine the truth? History,
594 theory, methods, and contrasting models. *Trees*. 28:643-655.
- 595 Choat B, Badel E, Burrett R, Delzon S, Cochard H, Jansen S (2016) Noninvasive Measurement of
596 Vulnerability to Drought-Induced Embolism by X-Ray Microtomography. *Plant Physiology*.
597 170:273-82.
- 598 Choat B, Drayton WM, Brodersen C, Matthews MA, Shackel KA, Wada H, McElrone AJ (2010)
599 Measurement of vulnerability to water stress-induced cavitation in grapevine: a comparison
600 of four techniques applied to a long-vesseled species. *Plant, Cell & Environment*. 33:1502-12.
- 601 Choat B, Jansen S, Brodrribb TJ, Cochard H, Delzon S, Bhaskar R, Bucci SJ, Feild TS, Gleason SM, Hacke
602 UG, Jacobsen AL, Lens F, Maherali H, Martinez-Vilalta J, Mayr S, Mencuccini M, Mitchell PJ,
603 Nardini A, Pittermann J, Pratt RB, Sperry JS, Westoby M, Wright IJ, Zanne AE (2012) Global
604 convergence in the vulnerability of forests to drought. *Nature*. 491:752-5.
- 605 Christman MA, Sperry JS, Adler FR (2009) Testing the 'rare pit' hypothesis for xylem cavitation
606 resistance in three species of *Acer*. *New Phytologist*. 182:664-674.
- 607 Cobb AR, Choat B, Holbrook NM (2007) Dynamics of freeze-thaw embolism in *Smilax rotundifolia*
608 (*Smilacaceae*). *American Journal of Botany*. 94:640-9.
- 609 Cochard H (2002) A technique for measuring xylem hydraulic conductance under high negative
610 pressures. *Plant, Cell & Environment*. 25:815-819.
- 611 Cochard H, Badel E, Herbette S, Delzon S, Choat B, Jansen S (2013) Methods for measuring plant
612 vulnerability to cavitation: a critical review. *Journal of Experimental Botany*. 64:4779-91.
- 613 Cochard H, Damour G, Bodet C, Tharwat I, Poirier M, Améglio T (2005) Evaluation of a new
614 centrifuge technique for rapid generation of xylem vulnerability curves. *Physiologia*
615 *Plantarum*. 124:410-418.
- 616 Cochard H, Delzon S, Badel E (2015) X-ray microtomography (micro-CT): a reference technology for
617 high-resolution quantification of xylem embolism in trees. *Plant, Cell & Environment*.
618 38:201-206.
- 619 Cochard H, Ewers F, Tyree M (1994) Water relations of a tropical vine-like bamboo (*Rhipidocladum*
620 *racemiflorum*): root pressures, vulnerability to cavitation and seasonal changes in embolism.
621 *Journal of Experimental Botany*. 45:1085-1089.
- 622 Cochard H, Herbette S, Barigah T, Badel E, Ennajeh M, Vilagrosa A (2010) Does sample length
623 influence the shape of xylem embolism vulnerability curves? A test with the Cavitron
624 spinning technique. *Plant, Cell & Environment*. 33:1543-52.
- 625 Cohen S, Bennink J, Tyree M (2003) Air method measurements of apple vessel length distributions
626 with improved apparatus and theory*. *Journal of Experimental Botany*. 54:1889-1897.

- 1
2
3 627 Dalla-Salda G, Fernández ME, Sergent A-S, Rozenberg P, Badel E, Martinez-Meier A (2014) Dynamics
4 628 of cavitation in a Douglas-fir tree-ring: transition-wood, the lord of the ring? *Journal of Plant*
5 629 *Hydraulics*. 1:005.
- 6 630 Duursma R (2017) An R implementation of the CAVITOPEN model
7 631 Duursma R, Choat B (2017) fitplc - an R package to fit hydraulic vulnerability curves. 2017. 4
8 632 Ennajeh M, Simoes F, Khemira H, Cochard H (2011) How reliable is the double-ended pressure sleeve
9 633 technique for assessing xylem vulnerability to cavitation in woody angiosperms? *Physiologia*
10 634 *Plantarum*. 142:205-10.
- 11 635 Ewers FW, Fisher JB (1989) Variation in vessel length and diameter in stems of six tropical and
12 636 subtropical lianas. *American Journal of Botany*:1452-1459.
- 13 637 Hacke UG, Venturas MD, MacKinnon ED, Jacobsen AL, Sperry JS, Pratt RB (2015) The standard
14 638 centrifuge method accurately measures vulnerability curves of long-vesselled olive stems.
15 639 *New Phytologist*. 205:116-27.
- 16 640 Holbrook NM, Burns MJ, Field CB (1995) Negative xylem pressures in plants: a test of the balancing
17 641 pressure technique. *Science*. 270:1193-1195.
- 18 642 Jacobsen AL, Pratt RB (2012) No evidence for an open vessel effect in centrifuge-based vulnerability
19 643 curves of a long-vesselled liana (*Vitis vinifera*). *New Phytologist*. 194:982-990.
- 20 644 Jansen S, Schuldt B, Choat B (2015) Current controversies and challenges in applying plant hydraulic
21 645 techniques. *New Phytologist*. 205:961-964.
- 22 646 Li Y, Sperry JS, Taneda H, Bush SE, Hacke UG (2008) Evaluation of centrifugal methods for measuring
23 647 xylem cavitation in conifers, diffuse- and ring-porous angiosperms. *New Phytologist*.
24 648 177:558-68.
- 25 649 Nardini A, Battistuzzo M, Savi T (2013) Shoot desiccation and hydraulic failure in temperate woody
26 650 angiosperms during an extreme summer drought. *New Phytologist*. 200:322-329.
- 27 651 Nolf M, Lopez R, Peters JM, Flavel RJ, Koloadin LS, Young IM, Choat B (2017) Visualization of xylem
28 652 embolism by X-ray microtomography: a direct test against hydraulic measurements. *New*
29 653 *Phytologist*. 214:890-898.
- 30 654 Ogle K, Barber JJ, Willson C, Thompson B (2009) Hierarchical statistical modeling of xylem
31 655 vulnerability to cavitation. *New Phytologist*. 182:541-554.
- 32 656 Pan R, Geng J, Cai J, Tyree MT (2015) A comparison of two methods for measuring vessel length in
33 657 woody plants. *Plant, Cell & Environment*. 38:2519-2526.
- 34 658 Pengxian Y, Feng M, Qing L, Rui A, Jing C, Guangyuan D A comparison of two centrifuge techniques
35 659 for constructing vulnerability curves: insight into the 'open-vessel' artifact. *Physiologia*
36 660 *Plantarum*. 0
- 37 661 Pockman WT, Sperry JS, Leary JW (1995) Sustained and significant negative water pressure in xylem.
38 662 *Nature*. 378:715.
- 39 663 Rodríguez-Calcerrada J, Li M, López R, Cano FJ, Oleksyn J, Atkin OK, Pita P, Aranda I, Gil L (2017)
40 664 Drought-induced shoot dieback starts with massive root xylem embolism and variable
41 665 depletion of nonstructural carbohydrates in seedlings of two tree species. *New Phytologist*.
42 666 213:597-610.
- 43 667 Sala A, Piper F, Hoch G (2010) Physiological mechanisms of drought-induced tree mortality are far
44 668 from being resolved. *New Phytologist*. 186:274-81.
- 45 669 Schneider CA, Rasband WS, Eliceiri KW (2012) NIH Image to ImageJ: 25 years of image analysis.
46 670 *Nature methods*. 9:671-675.
- 47 671 Schreiber SG, Hacke UG, Hamann A, Thomas BR (2011) Genetic variation of hydraulic and wood
48 672 anatomical traits in hybrid poplar and trembling aspen. *New Phytologist*. 190:150-160.
- 49 673 Sperry JS (1985) Xylem embolism in the palm *Rhapis excelsa*. *IAWA Journal*. 6:283-292.
- 50 674 Sperry JS, Christman MA, Torres-Ruiz JM, Taneda H, Smith DD (2012) Vulnerability curves by
51 675 centrifugation: is there an open vessel artefact, and are 'r' shaped curves necessarily invalid?
52 676 *Plant, Cell & Environment*. 35:601-10.

- 1
2
3 677 Sperry JS, Tyree MT (1988) Mechanism of water stress-induced xylem embolism. *Plant Physiology*.
4 678 88:581-7.
5 679 Tobin MF, Pratt RB, Jacobsen AL, De Guzman ME (2013) Xylem vulnerability to cavitation can be
6 680 accurately characterised in species with long vessels using a centrifuge method. *Plant*
7 681 *Biology*. 15:496-504.
8 682 Torres-Ruiz JM, Cochard H, Mayr S, Beikircher B, Diaz-Espejo A, Rodriguez-Dominguez CM, Badel E,
9 683 Fernandez JE (2014) Vulnerability to cavitation in *Olea europaea* current-year shoots: further
10 684 evidence of an open-vessel artifact associated with centrifuge and air-injection techniques.
11 685 *Physiologia Plantarum*. 152:465-74.
12 686 Torres-Ruiz JM, Cochard H, Mencuccini M, Delzon S, Badel E (2016) Direct observation and modelling
13 687 of embolism spread between xylem conduits: a case study in Scots pine. *Plant, Cell &*
14 688 *Environment*. 39:2774-2785.
15 689 Torres-Ruiz JM, Jansen S, Choat B, McElrone AJ, Cochard H, Brodribb TJ, Badel E, Burrett R, Bouche
16 690 PS, Brodersen CR (2015) Direct X-ray microtomography observation confirms the induction
17 691 of embolism upon xylem cutting under tension. *Plant Physiology*. 167:40-43.
18 692 Torres-Ruiz JM, Cochard H, Choat B, Jansen S, López R, Tomášková I, Padilla-Díaz CM, Badel E, Burrett
19 693 R, King A (2017) Xylem resistance to embolism: presenting a simple diagnostic test for the
20 694 open vessel artefact. *New Phytologist*. 215:489-499.
21 695 Tyree MT, Dixon MA (1986) Water stress induced cavitation and embolism in some woody plants.
22 696 *Physiologia Plantarum*. 66:397-405.
23 697 Tyree MT, Sperry JS (1988) Do woody plants operate near the point of catastrophic xylem
24 698 dysfunction caused by dynamic water stress? : answers from a model. *Plant Physiology*.
25 699 88:574-80.
26 700 Tyree MT, Zimmermann MH (2002) Hydraulic architecture of whole plants and plant performance
27 701 Xylem structure and the ascent of sap. Springer, pp 175-214.
28 702 Urli M, Porte AJ, Cochard H, Guengant Y, Burrett R, Delzon S (2013) Xylem embolism threshold for
29 703 catastrophic hydraulic failure in angiosperm trees. *Tree Physiology*. 33:672-83.
30 704 Venturas MD, MacKinnon ED, Dario HL, Jacobsen AL, Pratt RB, Davis SD (2016) Chaparral shrub
31 705 hydraulic traits, size, and life history types relate to species mortality during California's
32 706 historic drought of 2014. *PloS one*. 11:e0159145.
33 707 Wang R, Zhang L, Zhang S, Cai J, Tyree MT (2014) Water relations of *Robinia pseudoacacia* L.: do
34 708 vessels cavitate and refill diurnally or are R-shaped curves invalid in *Robinia*? *Plant, cell &*
35 709 *environment*. 37:2667-2678.
36 710 Wheeler JK, Huggett BA, Tofte AN, Rockwell FE, Holbrook NM (2013) Cutting xylem under tension or
37 711 supersaturated with gas can generate PLC and the appearance of rapid recovery from
38 712 embolism. *Plant, Cell & Environment*. 36:1938-1949.
39
40
41 713
42
43
44 714
45
46
47
48
49
50
51
52
53
54
55
56
57
58
59
60

1
2
3 715 **Figure legends**
4

5
6 716 **Figure 1.** Distribution of PLC in air-injected branches of *H. dactyloides* (black circles) and *H.*
7
8 717 *leucoptera* (open circles) at different positions from the injected end. Vertical bars represent the
9
10 718 standard error. Dashed lines indicate the two sample lengths used for the centrifuge methods, 14 cm
11
12 719 and 27 cm and dot lines indicate their respective half sample length.

13
14
15 720 **Figure 2.** Xylem vulnerability to embolism curves and 95% confidence intervals (grey shaded areas)
16
17 721 of *Hakea dactyloides* (left panels) and *Hakea leucoptera* (right panels) obtained with two methods to
18
19 722 induce cavitation in the xylem, bench dehydration and centrifuge force and three methods to
20
21 723 measure the loss of conductivity, flowmeter (close circles), in situ flow method (open circles) and X-
22
23 724 ray microCT visualisation (red triangles). Vertical solid lines indicate P_{50} and vertical dashed lines
24
25 725 indicate the 95% confidence interval for P_{50} . Horizontal dashed lines indicated native xylem
26
27 726 embolism measured in the field. Two rotor sizes, 14 cm and 27 cm, were used in the static
28
29 727 centrifuge, and water flow in the whole segment or only in the central part was measured (see
30
31 728 methods for details).

32
33
34 729 **Figure 3.** Transverse slices from X-ray microtomography (X-ray micro-CT) scans of branches of *Hakea*
35
36 730 *leucoptera* (maximum vessel length = 25 ± 5 cm) scanned at three positions before spinning (left
37
38 731 column) and after spinning in the centrifuge at 5, 7 and 9 MPa. Embolized vessels appear as black
39
40 732 and water-filled conduits appear as grey. The estimated percent loss of conductivity (PLC) is shown
41
42 733 in each picture. Scale bar, 1 mm.

43
44
45 734 **Figure 4.** Simulations with the CAVITOPEN model of the effect of threshold of embolism formation
46
47 735 (MPa) of cut open vessels (A), maximum vessel length (cm) (B), and rotor size (cm) (C) on xylem
48
49 736 vulnerability to embolism curves generated with centrifugation. In red, vulnerability curve of close
50
51 737 vessels at both ends. (D) The CAVITOPEN model was fit to measurements in *H. leucoptera* using
52
53 738 numerical optimization to estimate all four parameters: water potential at 50% loss of conductivity
54
55
56
57
58
59
60

1
2
3 739 (P_{50}), slope of the vulnerability curve (S_{50}), maximum vessel length (L_{max}) and threshold of embolism
4
5 740 formation of cut open vessels (P_{open}). Circles represent the values obtained in our study with the
6
7 741 static centrifuge, 27 cm rotor in *H. leucoptera* when flow was measured in the whole segment (see
8
9 742 Methods for details); grey solid line is the fitted curve with the CAVITOPEN model; black solid line
10
11 743 represent the curve after correction and orange dashed line is the reference curve obtained with
12
13 744 bench dehydration for the species.

14
15
16 745
17
18
19
20
21
22
23
24
25
26
27
28
29
30
31
32
33
34
35
36
37
38
39
40
41
42
43
44
45
46
47
48
49
50
51
52
53
54
55
56
57
58
59
60

For Peer Review

1
2
3
4
5
6
7
8 1 **Title:** Mitigating the open vessel artefact in centrifuge based measurement of embolism resistance

9
10 2 **Running head:** Mitigating artefacts in vulnerability curves

11
12
13 3

14
15 4

16
17 5 Rosana López^{1,2}, Markus Nolf³, Remko A Duursma³, Eric Badel¹, Richard J Flavel⁴, Hervé Cochard¹,

18
19 6 Brendan Choat³

20
21
22 7

23
24 8 1- Université Clermont Auvergne, INRA, PIAF, Clermont-Ferrand, France.

25
26 9 2- Sistemas y Recursos Naturales, Universidad Politécnica de Madrid, Madrid, Spain.

27
28 10 3- Hawkesbury Institute for the Environment, Western Sydney University, Richmond, NSW, Australia.

29
30 11 4- School of Environmental and Rural Science, University of New England, Armidale, NSW, Australia.

31
32
33 12

34
35 13 **Corresponding author details:**

36
37 14 Dr. Rosana López

38
39 15 e-mail: rosana.lopez@upm.es

40
41
42 16 phone: +34 655868659

43
44
45 17 Address: ETSI Montes, Forestal y del Medio Natural. C/ José Antonio Novais, 10. 28040 Madrid

46
47
48 18

49
50 19

51
52
53 1

Abstract (300 words max)

Con formato: Español (España)

Centrifuge-based techniques to assess xylem vulnerability to embolism are increasingly being used, although we are yet to reach a consensus on the nature and extent of artefactual embolism observed in some angiosperm species. In particular, there is disagreement over whether these artefacts influence both the spin (Cavitron) and static versions of the centrifuge technique equally.

We tested two methods for inducing embolism: bench dehydration and centrifugation. We used three methods to measure the resulting loss of conductivity: gravimetric flow measured in bench-dehydrated and centrifuged samples (static centrifuge), in situ flow measured under tension during spinning in the centrifuge (Cavitron), and direct imaging using X-ray microCT observations in stems of two species of *Hakea* that differ in vessel length.

Con formato: Fuente: Cursiva

Both centrifuge techniques were prone to artefactual embolism in samples with maximum vessel length longer, or similar, to the centrifuge rotor diameter. Observations with microCT indicated that this artefactual embolism occurred in the outer most portions of samples. The artefact was largely eliminated if flow was measured in an excised central part of the segment in the static centrifuge or starting measurements with the Cavitron at pressures lower than the threshold of embolism formation in open vessels. The simulations of loss of conductivity in centrifuged samples with a new model, CAVITOPEN, confirmed that the impact of open vessels on the vulnerability to embolism curve was higher when vessels were long, samples short and when embolism is formed in open vessels at less negative pressures. This model also offers a robust and quantitative tool to test and correct for artefactual embolism at low xylem tensions.

Keywords

Vulnerability to embolism, xylem embolism, drought, centrifuge technique, Cavitron, X-Ray microCT, CAVITOPEN.

44 Introduction

45 Xylem water transport is dependent upon water held in a metastable state of water; evaporation of
46 water from the leaf cell walls generates tension, which is transmitted through the water column to
47 the roots. Water under tension is prone to cavitation, i.e. the abrupt transition from a metastable
48 liquid to a gas, resulting in the formation of gas emboli that block the xylem conduits and impairs
49 water transport (Tyree and Sperry 1988). As tension in the xylem sap increases, for example during
50 drought, so does the probability of embolism formation. During severe or prolonged droughts,
51 hydraulic failure can result in the complete loss of hydraulic conductance in the xylem and subsequent
52 canopy dieback, or whole plant death (Brodribb and Cochard 2009; Nardini et al. 2013; Rodríguez-
53 Calcerrada et al. 2017; Urli et al. 2013; Venturas et al. 2016). Hydraulic failure is now considered a
54 principal cause of drought-induced plant mortality and forest die off (Choat et al. 2012; Sala et al.
55 2010). The projected rise in global mean temperature and frequency of extreme climate events over
56 the next century will impact forest ecosystems and shift species distribution ranges. In this sense,
57 resistance to embolism has emerged as a crucial parameter to understanding species ecology,
58 differences in water use strategies, and for predicting future mortality events (Brodribb 2017).

59 Xylem resistance to embolism is usually characterized with a vulnerability curve, showing the decrease
60 in hydraulic conductivity as a function of the xylem tension. Since the publication of the first
61 vulnerability curves for woody plants were published in 1985 (Sperry 1985) and 1986 (Tyree and Dixon
62 1986), a number of techniques that allow for more rapid measurement of vulnerability have been
63 introduced (see Cochard et al. (2013) for a detailed review). However, although the time required for
64 construction of a vulnerability curve has been dramatically reduced, recent work suggests that some
65 of these methods are prone to experimental artefact (Choat et al. 2010; Cochard et al. 2010; Sperry
66 et al. 2012; Torres-Ruiz et al. 2014). This has led to re-examination of methodology used to measure
67 vulnerability to embolism (Jansen et al. 2015).

1
2
3
4
5
6
7
8 68 The most straightforward technique for inducing embolism is bench dehydration, wherein whole
9
10 69 plants or long branches are gradually dehydrated to various xylem tensions and hydraulic conductivity
11
12 70 of excised segments is measured gravimetrically before and after removing air from embolised
13
14 71 conduits (Sperry and Tyree 1988; Tyree and Zimmermann 2002). Bench dehydration relies on natural
15
16 72 desiccation of plant tissues and is therefore considered as the best reference method with which to
17
18 73 validate other techniques (Cochard et al. 2013; Ennajeh et al. 2011; Sperry et al. 2012). This method
19
20 74 is not completely free of artefacts and issues associated with disequilibrium in water potential within
21
22 75 a stem, blockage of flow by resin/mucilage (Cobb et al. 2007), and excision of samples under tension
23
24 76 can all alter the vulnerability curve significantly (Wheeler et al., 2013). Although most of these issues
25
26 77 can be minimised by adoption of suitable protocols (eg. Torres-Ruiz et al., 2015), the bench
27
28 78 dehydration technique requires several days and a substantial amount of plant material to obtain a
29
30 79 vulnerability curve for one species. As such, Holbrook et al. (1995) and Pockman et al. (1995) proposed
31
32 80 the use of a centrifugal force to create a defined negative pressure in the xylem sap of excised plant
33
34 81 stems, allowing for rapid and consistent generation of vulnerability curves. Pockman et al. (1995)
35
36 82 constructed vulnerability curves for several species by comparing the hydraulic conductivity before
37
38 83 and after spinning branches with their ends exposed to air, removing segments at both ends before
39
40 84 measuring conductivity in the remaining, middle section of the sample. Alder et al. (1997) modified
41
42 85 this technique with a centrifuge rotor designed to keep the segment ends immersed in water during
43
44 86 spinning, allowing the conductivity of a single segment to be remeasured at different tensions to
45
46 87 create an entire vulnerability curve for a single sample. This important innovation allowed repeated
47
48 88 measurements to be made on the same plant material, reducing the number of samples required for
49
50 89 construction of a curve and strengthening the results statistically. Finally, Cochard (2002), Cochard et
51
52 90 al. (2005) and Li et al. (2008) further modified the centrifuge method and designed new rotors which
53
54 91 allowed measuring the conductivity of the segment while it is spinning and under tension. This further
55
56 92 increased the efficiency of measurement and allowed for flow measurements to be made under
57
58 93 tension.

1
2
3
4
5
6
7
8 94 Although centrifuge based techniques induce embolism by increasing tension in sample xylem, the
9
10 95 patterns of embolism spread through the sample may differ from a naturally dehydrated sample (Cai
11
12 96 et al. 2010). The tension profile in the centrifuged segment is highest in the axis of rotation (i.e. in the
13
14 97 middle section of the segment) and declines towards the segment ends (Cochard et al. 2005), while
15
16 98 during natural dehydration the tension profile across the segment is expected to remain
17
18 99 approximately constant (Cai et al. 2010). Nevertheless, the vulnerability curves generated by
19
20 100 centrifugation agree well with the bench-top method in conifers and short-vesseled angiosperm
21
22 101 species (Alder et al. 1997; Cochard et al. 2005; Cochard et al. 2010; Li et al. 2008). In contrast,
23
24 102 inconsistent results have been obtained for species with long vessels, specifically those in which a
25
26 103 significant number of vessels in the sample are longer than the centrifuge rotor (Choat et al. 2010;
27
28 104 Jacobsen and Pratt 2012; Sperry et al. 2012; Torres-Ruiz et al. 2014).

29 105 Since 2005 the number of vulnerability curves constructed by centrifugation has increased
30
31 106 exponentially (see Fig. 3 in Cochard et al. (2013)). Accordingly, considerable effort has been devoted
32
33 107 to testing and validation of centrifuge techniques, whether measuring the flow gravimetrically after
34
35 108 spinning (static centrifuge method), or while centrifuging (Cavitron method). However, we are yet to
36
37 109 reach a consensus on the nature and extent of artefactual embolism observed with centrifuge
38
39 110 techniques. In particular, there is disagreement over whether these artefacts influence both spin
40
41 111 (Cavitron rotor) and static versions of the centrifuge technique equally (Hacke et al. 2015; Sperry et
42
43 112 al. 2012). In recent years, the application of x-ray computed microtomography (microCT) to the study
44
45 113 of plant hydraulics has emerged as a potentially powerful tool to validate hydraulic techniques. In
46
47 114 addition to providing a non-invasive assay of xylem function, it allows for analyses of spatial and
48
49 115 temporal patterns of embolism formation (Brodersen et al. 2013; Choat et al. 2016; Dalla-Salda et al.
50
51 116 2014; Torres-Ruiz et al. 2016).

52
53
54
55
56
57
58
59 117 In this study we evaluated the performance of both centrifuge techniques against bench dehydration
60 118 in order to examine possible discrepancies associated with each technique. First, we tested two

1
2
3
4
5
6
7
8 119 methods for inducing embolism: bench dehydration and centrifugation. We then tested three ways of
9
10 120 measuring the resulting loss of conductivity: gravimetric flow measured in bench-dehydrated and
11
12 121 centrifuged samples (static centrifuge), *in situ* flow measured under tension during spinning in the
13
14 122 centrifuge (Cavitron), and direct imaging using X-ray microCT observation. All experiments were
15
16 123 carried out with two species of the genus *Hakea* that differ in vessel length. *H. dactyloides* is a short
17
18 124 vesseled species with maximum vessel length shorter than 14 cm, whereas *H. leucoptera* has longer
19
20 125 vessels and maximum vessel length is ca. 25 cm. Additionally, we compared results obtained using
21
22 126 two rotor diameters (14 and 27 cm) to assess the effect of sample length, and measured hydraulic
23
24 127 flow both in the whole, spun segments and excised middle sections. Spatial patterns of embolism
25
26 128 within samples were visualized with X-ray microCT after centrifugation in order to provide further
27
28 129 insight into potential discrepancies. Finally, a new model, CAVITOPEN was developed to simulate the
29
30 130 effect of vessel and sample lengths on centrifuge estimates of embolism resistance. We hypothesized
31
32 131 that i) both centrifuge techniques, the static centrifuge and the cavitron, are prone to similar artefacts
33
34 132 when constructing vulnerability curves of long-vesseled species; ii) the shape of the vulnerability curve
35
36 133 of centrifuged samples will depend on the amount of cut open vessels; iii) image techniques and
37
38 134 standard flow measurements will produce similar vulnerability curves.

135

136 **Material and methods**

137 *Plant Material*

138 Experiments were carried out on branch material of two diffuse-porous species of the same genus
139 exhibiting different vessel lengths, *Hakea dactyloides* (Gaertn.) Cav. and *Hakea leucoptera* R. Br.
140 Branches were sampled from natural populations of *H. dactyloides* at Mount Banks (33° 34' 46'' S,
141 150° 21' 56'' E; NSW, Australia) and *H. leucoptera* at Binya State Forest (34° 11' 16'' S, 146° 16' 13'' E;
142 NSW, Australia) from May to September 2016 (late autumn-winter in the South Hemisphere). Sun

6

1
2
3
4
5
6
7
8 143 exposed branches of 1.5-2.0 m length were collected in the field in the early morning and immediately
9 144 placed in black plastic bags with moistened paper towels to prevent transpiration with their cut ends
10
11 145 covered with Parafilm. In the laboratory they were kept at 4 °C until measured.

12
13
14 146 *Midday xylem water potential in the field and Native embolism*

15
16 147 Midday xylem water potential was measured in the field in November 2015, February 2016 and June
17 148 2016. Two leaves of five plants per species were covered with aluminium foil and sealed with a plastic
18
19 149 bag 1 hour before excision and measurement with a pressure chamber (PMS Instrument Co., Albany,
20
21 150 OR, USA).

22
23 151 Native embolism was determined in current-year, one-year and two-year old segments of 5 branches
24
25 152 per species to ensure that the effects of previous natural water stress were minimised. ~~due to~~Note
26
27 153 that segments containing 1-year and 2-year-old growth were necessary to fit in the 27 cm rotor of the
28
29 154 centrifuge. ~~Measuring native embolism we also wanted and~~ to control for sample collection date
30
31 155 because branches were cut at different times during late autumn-winter 2016 to avoid long storage.

32 156 Branch proximal end was cut underwater to release tension for 30 min (Torres-Ruiz et al. 2015;
33
34 157 Wheeler et al. 2013) and then the branch was progressively recut under water to segments 50 mm
35
36 158 long. Note that at least twice the maximum vessel length was removed from the cut end after tension
37
38 159 relaxation. Thereafter, the edges of these segments were trimmed using a razor blade. Initial
39
40 160 conductivity (K_i) was measured in 50 mm long segments with filtered, degassed 2 mmol KCl solution
41
42 161 at low pressure (≤ 4 kPa) with a liquid flowmeter (LiquiFlow L13-AAD-11-K-10S; Bronkhorst High-Tech
43
44 162 B.V., Ruurlo, the Netherlands). The segments were then flushed with the same solution at a minimum
45
46 163 of 0.20 MPa for 15 min to remove embolism and subsequently determine maximum hydraulic
47
48 164 conductivity (K_{max}). The native percentage loss of conductivity (PLC) was calculated for each segment
49
50 165 as:

51
52
53
54
55
56
57
58
59
60 166 $PLC = 100 \times (1 - K_i / K_{max})$ (equation 1)

1
2
3
4
5
6
7
8 167 Specific hydraulic conductivity (K_s) was calculated dividing K_{max} by the xylem cross-sectional area
9 168 (average distal and proximal xylem area measured with a calliper).

10
11
12 169 *Maximum vessel length and vessel length distribution*

13
14 170 Ten branches per species were sampled from the same plants as used for hydraulic measurements to
15
16 171 determine maximum vessel length with the air perfusion technique (Ewers and Fisher 1989). Once in
17
18 172 the lab, 60 cm long segments were flushed for 1 h with degassed, filtered 2 mmol KCl solution at 0.18-
19
20 173 0.20 MPa to remove any embolism. Then each segment was infiltrated with compressed air at 0.05
21
22 174 MPa at its distal end with an aquarium air pump while the basal end was repeatedly shortened by 2
23
24 175 cm under water until air bubbles emerged. The remaining sample length was assumed as maximum
25
26 176 vessel length.

27 177 An estimate of the amount of vessels longer than the centrifuge rotor diameter and longer than half
28
29 178 the rotor diameter (open to centre vessels) was assessed in four branches of *H. dactyloides* and five
30
31 179 branches of *H. leuoptera* by measuring the decrease in PLC after air injection (Cochard et al. 1994;
32
33 180 Torres-Ruiz et al. 2014). Briefly, 35 cm long segments were flushed as described above to remove
34
35 181 embolism. Then, tubing was attached to the distal end of these segments and compressed air was
36
37 182 injected into the samples at 0.1 MPa for 10 min using a pressure chamber. This pressure was sufficient
38
39 183 to empty the open vessels but not high enough to move water through wet pit membranes between
40
41 184 adjacent vessels (Ewers and Fisher, 1989). PLC was determined in 3 cm long segments across the
42
43 185 sample as described for native embolism. At the injection point, PLC is close to 100% because all the
44
45 186 vessels are air filled and progressively decrease to 0 for a length longer than the longest vessel in the
46
47 187 sample. The PLC at each distance from the injection point corresponds to the percentage of
48
49 188 contribution to flow from vessels longer than this distance. If all the vessels were of equal diameter,
50
51 189 this percentage would correspond to the number of vessels longer than the distance from the injection
52
53 190 point. In this case of the two *Hakea* species used are diffuse porous and vessel diameters within the
54
55 191 same sample did not vary greatly. Thus the curves in Fig. 1 represent a ~~good~~ proxy of vessel distribution

Con formato: Fuente: Cursiva

1
2
3
4
5
6
7
8 192 of the two species, although not as accurate as anatomy, and allow to estimate the amount of open
9 193 vessels from a certain cut point.

12 194 *Bench dehydration technique*

14 195 Branches were dehydrated gradually in the laboratory at ca. 23 °C. Xylem water potential (Ψ_x) was
15 196 measured with a pressure chamber (PMS Instrument Co., Albany, OR, USA) in bagged leaves (wrapped
16 197 with aluminium foil and a plastic bag at least 1 h before sampling). When the target Ψ_x to construct
17 198 the VC was reached, branches were sealed into a plastic bag with moistened paper towels for 1 h to
18 199 equilibrate Ψ_x . Water potential was measured again in two bagged leaves of the same branchlet to
19 200 confirm homogeneous Ψ_x in the sample. The Ψ_x of the sample was considered equilibrated if the
20 201 difference between the three Ψ_x (one measured before sealing the branch and two measured after
21 202 equilibration) was not higher than 0.1 MPa. Afterwards tension was released for 30 minutes by cutting
22 203 the branch proximal end under water and PLC was determined in one-year-old segments as for native
23 204 embolism. Vulnerability curves were generated by plotting PLC against Ψ_x . For *H. leucoptera* 7
24 205 branches were dehydrated and 4 different branchlets per branch were measured at different Ψ_x to
25 206 construct the vulnerability curve and for *H. dactyloides* we used 12 branches and two branchlets per
26 207 branch. All branchlets were far apart (at least four branch orders) and after collection the cutting
27 208 surface was covered with parafilm to avoid air entry in the rest of the sample.

39 209 *Centrifuge techniques*

41 210 We compared two centrifuge techniques: i) the static centrifuge method described by Alder et al.
42 211 (1997) and ii) the *in situ* flow technique (Cavitron (Cochard 2002; Cochard et al. 2005)). In the static
43 212 centrifuge two different sizes of custom-built rotors, 14 cm and 27 cm, were used to test the effect of
44 213 segment length and fraction of open vessels. All hydraulic conductivity measurements were
45 214 performed using filtered, degassed 2 mmol KCl solution and a flow meter (see Native embolism
46 215 section).

1
2
3
4
5
6
7
8 216 Static centrifuge measurements were carried out on 20 branches per species. Branches were trimmed
9
10 217 under water and both ends were shaved to a final length of 14 or 27 cm. The initial hydraulic
11
12 218 conductivity was measured as described above (see Native embolism section) with a pressure head of
13
14 219 7.5 kPa. Subsequently, 14-cm long branches were spun in the centrifuge (Sorvall RC 5C Plus) for 5
15
16 220 minutes at increasing pressure steps. Foam pads saturated with the solution used for measurements
17
18 221 were placed in the reservoirs of the rotor to maintain sample ends in contact with the solution even
19
20 222 when the rotor was stopped (Tobin et al. 2013). After each step, samples were removed and K_h was
21
22 223 measured on the whole segment as described for native embolism. In the 27cm-long branches we
23
24 224 modified the single spin method (Hacke et al. 2015) so that two measurements were made in each
25
26 225 centrifuged segment. The initial K_h was measured before spinning in the 27-cm long sample. After
27
28 226 spinning, K_h was measured on the whole segment and the first PLC was calculated. Subsequently, a 4
29
30 227 cm-long segment was cut from the middle section and its K_h was measured. The second PLC was
31
32 228 determined in this 4 cm-long segment after flushing to obtained the maximum K_h (K_{max}) as described
33
34 229 for native embolism.

35
36 230 *In situ* flow centrifuge measurements (Cavitron technique) were carried out on six branches per
37
38 231 species using a modified bench top centrifuge (H2100R, Cence Xiangyi, Hunan, China). For the static
39
40 232 centrifuge, samples were trimmed under water to a length of 27 cm to fit in the rotor. Initial
41
42 233 conductivity, K_i , was determined at a xylem pressure of -0.5 MPa in *H. dactyloides* and 1.5 MPa in *H.*
43
44 234 *leucoptera*. The xylem pressure was then lowered stepwise by increasing the rotational velocity, and
45
46 235 K_h was again determined while the sample was spinning. The PLC at each pressure step was quantified
47
48 236 as

$$45 \quad 237 \quad PLC = 100 \times (1 - K_h / K_i). \quad (\text{equation 2})$$

49
50
51
52
53
54
55
56
57
58
59
60 238 *X-ray microCT imaging*

239 A subset of branches of *H. leucomelaena* was transported to the University of New England in Armidale
240 (NSW, Australia). They were gradually dehydrated to five different xylem water potentials ranging
241 from -4.8 MPa to -9 MPa as for the bench dehydration method. After measuring Ψ_x , tension was
242 relaxed by cutting the proximal end of the branch under water leaving it submerged for 30 minutes.
243 Then the branch was sequentially cut back under water and finally 10-mm-long segments were excised
244 under water from current-year shoots, wrapped in Parafilm, inserted into a plexiglass tube and then
245 placed in an X-ray microtomography system (GE-Phoenix V|tome|xS, GE Sensing & Inspection
246 Technologies, Wunstorf, Germany) to visualize embolized vessels. Another subset of branches of *H.*
247 *leucomelaena* was centrifuged to five (-5, -6, -7, -8, -9 MPa) and three (-5, -6, -7 MPa) different water
248 potentials in the static centrifuge using 27 cm and 14 cm long segments, respectively. They were
249 immediately submerged in liquid paraffin wax and preserved at 4 °C for three days until measured in
250 the same facility (Cochard et al. 2015). Seven branches of *H. dactyloides* were also centrifuged at four
251 (-3, -4, -5, -6 MPa) and three (-3, -4, -5 MPa) water potentials with the 27 and 14 cm rotors,
252 respectively, following the same protocol. One branch of *H. leucomelaena* was prepared as the
253 centrifuged samples but was not spun in the centrifuge to detect any possible artefact due to sample
254 preparation. All samples were scanned at the middle of the sample. Additionally, in three 27 cm long
255 samples we scanned at 6 cm and 12 cm from the axis of rotation to examine embolism profiles across
256 a sample.

257 X-ray scan settings were 90 kV and 170 mA, and 1800 projections, 600 ms each, were acquired during
258 the 360° rotation of the sample. The resultant images covered the whole cross section of the sample
259 in 8.7 mm length with a spatial resolution of 8.7 μm per voxel. At the end of the scan, the sample was
260 cut back to 30 mm length, injected with air at >1 MPa pressure and rescanned at the same location as
261 before to visualize all empty vessels in the fully embolized cross section. After three-dimensional
262 reconstruction with Phoenix datos|x2 Reconstruction Version 2.2.1-RTM (GE Sensing & Inspection
263 Technologies, Wunstorf, Germany), volumes were imported into ImageJ 1.49k (Schneider et al. 2012).
264 A median Z projection of c. 100 μm along the sample axis was extracted from the middle of the scan

1
2
3
4
5
6
7
8 265 volumes following the protocol in Nolf et al. (2017). PLC of each sample was estimated calculating the
9
10 266 theoretical hydraulic conductance based on the conduit dimensions of embolized and functional
11
12 267 vessels (Choat et al. 2016). To measure conduit dimensions, a radial sector of the transverse section
13
14 268 was selected in the same microCT scan and all their embolized vessels were measured manually. The
15
16 269 image of this sector was then binarized so the dimensions of the selected embolized vessels matched
17
18 270 with the manually drawn vessels. This threshold value was then used for binarizing the image of the
19
20 271 whole cross section and all the embolized vessels were measured using the Analyse Particles function
21
22 272 in Image J. Theoretical specific hydraulic conductivity (K_{sth}) was calculated as:

$$23 \quad K_{sth} = \frac{\sum \left(\frac{D^4 \pi}{128 \eta} \cdot \frac{\Delta p}{\Delta x} \right)}{A} \quad \text{(equation 3)}$$

24
25 274
26 275 Where D is the equivalent circular vessel diameter based on vessel area, η viscosity of water, $\Delta p/\Delta x$
27
28 276 pressure gradient per xylem length, A xylem cross-sectional area.
29

30 277
31 278 The current theoretical specific hydraulic conductivity (K_{sth}) for each sample was calculated by
32
33 279 subtracting the summed specific hydraulic conductivity of embolized vessels from the $K_{sth(max)}$ of that
34
35 280 sample, calculated as the K_{sth} of the sample after air injection. The pressure gradient used for
36
37 281 calculations of K_{sth} was similar to the pressure gradient used in the hydraulic measurements, 0.06 MPa
38
39 282 m^{-1} .

40 283 41 42 284 *Vulnerability curve fitting and statistical analysis*

43
44 285 Vulnerability curves were fitted using a Weibull function (Ogle et al. 2009) in R 3.2.0 (R Core Team,
45
46 286 2015) using the fitplc package (Duursma and Choat 2017). Confidence intervals of P_{12} , P_{50} and P_{88} (Ψ_x
47
48 287 at 12, 50 and 88 % loss of conductivity, respectively) and the slope of the curve at 50% loss of
49
50 288 conductivity (S_{50}) were used to compare between methods. Confidence intervals (CI) for the bench

289 dehydration and the static centrifuge techniques were obtained using bootstrap resampling (999
 290 replicates). Methods were considered to be statistically different if the 95% CIs did not overlap.

291 Differences in native embolism and specific initial conductivity between sampling dates were tested
 292 with a one-way ANOVA. Means were compared using a Tukey test at 95% confidence. Vulnerability
 293 curve parameters across methods were compared at the Ψ_x corresponding with three levels of loss
 294 of conductivity: 12%, 50% and 88% (P_{12} , P_{50} and P_{88} , respectively) and the slope of the VC at 50% loss
 295 of conductivity (S_{50}).

296 *CAVITOPEN- simulation of the effect of open vessels in a centrifuged sample*

297 To disentangle the ~~combined~~ effects of centrifugation on 'true' vessel embolism at the centre of the
 298 samples, where more vessels are closed at both ends and tension is maximum, from draining of open
 299 vessels at both sample ends a new model, CAVITOPEN, was developed. In a centrifuged sample, the
 300 variation of xylem pressure (P) with distance from the axis of rotation (r) is given by the following
 301 equation (Alder et al. 1997):

$$302 \quad dP/dr = \rho\omega^2r \quad (\text{equation 4})$$

303 where ρ is the density of water, and ω the angular velocity.

304 Integrating this equation from R (distance from the axis of rotation to the water reservoir) we can
 305 obtain the pressure at r (P_r):

$$306 \quad P_r = 0.5 \rho\omega^2(R^2 - r^2) \quad (\text{equation 5})$$

307 The effect of vessel length on 'true' vessel embolism in a spun sample has already been modelled by
 308 Cochard et al (2005). Briefly, if the vessels are infinitely long, the VC obtained by centrifugation should
 309 yield the correct P_{50} value. When the vessels are infinitely short the P_{50} value is underestimated due
 310 to the variation of xylem pressure inside the spun sample (eq. 4) and the consequent gradient of
 311 embolism along the sample: xylem pressure is minimum in the middle of the sample and null at the

1
2
3
4
5
6
7
8 312 extremities (eq. 5). Since the loss of conductivity is measured on the whole sample, an
9
10 313 underestimation of the degree of embolism in the middle of the sample is predicted. This effect of
11
12 314 vessel length was further tested with the CAVITOPEN model and found marginal, i.e. the shift in the
13
14 315 VC was negligible, compared to the draining effect. For sake of simplicity, this effect was no longer
15
16 316 considered in the simulations. To simulate the draining effect at both sample ends, we first
17
18 317 hypothesized that vessel ends follow a logarithmic distribution following the vessel length probability
19
20 318 density function proposed by Cohen et al. (2003) and assuming vessel ends uniformly distributed
21
22 319 across the length of the sample:

$$22 \quad N_x = N_0 \cdot \exp(-x/L_{max}) \quad \text{(equation 6)}$$

23
24 321 where N_x is the number of open vessels at the distance x from sample ends, N_0 the total number of
25
26 322 vessels and L_{max} the maximum vessel length.

27
28 323 The second assumption of the model is that open vessels drain when the minimum pressure in the
29
30 324 vessel exceeds a threshold value P_{open} . Because of the quadratic distribution of the pressure in the
31
32 325 sample, vessels having their end wall located closer to the sample ends, i. e. further from the centre
33
34 326 of rotation, will drain at a higher rotational velocity.

35
36 327 The branch segment was discretised in 0.1 mm thick sections arranged in serial. The xylem pressure
37
38 328 in the middle of the segment was set to a pressure varying from 0 to -12 MPa in 1 MPa steps. The
39
40 329 model then computes the pressure at steady state in each 0.1 mm section and determines the PLC
41
42 330 caused by 'true' embolism (non-open vessels) and by draining (open vessels). Finally, the PLC of the
43
44 331 whole segment is computed which enables the construction of the vulnerability curve. We tested the
45
46 332 model for different theoretical L_{max} values and the 4 rotors sizes used in our experiments. To validate
47
48 333 the model we used the values of PLC obtained for *H. leucoptera* in the static centrifuge with the 27 cm
49
50 334 rotor. The CAVITOPEN model was fit to the measurements using constrained numerical optimization

335 to estimate four parameters: P_{50} , S_{50} , L_{max} and P_{open} . All routines were implemented as an R package
336 (available from (Duursma 2017)).

337 Results

338 *Native embolism and minimum xylem water potential in the field.*

339 Midday xylem water potential decreased from -1.02 to -1.51 MPa in *H. dactyloides* and from -1.35 to
340 -2.62 MPa in *H. leucoptera* from November 2015 to February 2016. In June 2016, the water potential
341 was -1.16 MPa in *H. dactyloides* and -1.42 MPa in *H. leucoptera*. Native embolism remained low in
342 both species across the sampling dates. We measured higher PLC in two-year-old branch segments (<
343 13 %) than in current year growth (< 2 %) in *H. leucoptera* whereas in *H. dactyloides* native embolism
344 was lower than 2% in all samples. Maximum xylem specific conductivity (K_{smax}) was $0.87 \pm 0.10 \text{ kg m}^{-1}$
345 $\text{s}^{-1} \text{ MPa}^{-1}$ in *H. leucoptera* and $1.29 \pm 0.09 \text{ kg m}^{-1} \text{ s}^{-1} \text{ MPa}^{-1}$ in *H. dactyloides* (mean \pm sd). No significant
346 differences in native PLC or K_s ($P > 0.05$; Table S1) were detected between sampling dates.

347 *Maximum vessel length and vessel length distribution*

348 Maximum vessel length as determined by air injection was 25 cm (standard deviation, sd = 5) in *H.*
349 *leucoptera* and 10 cm (sd = 3) in *H. dactyloides*. Air injected branches of *H. dactyloides* showed 17%
350 PLC at 7 cm from the injection point, 5% at 14 cm and less than 1% at 28 cm, whereas in *H. leucoptera*
351 the PLC was always higher, 50%, 25%, and 5% at 7, 14 and 28 cm respectively (Fig. 1). Thus the number
352 of open vessels at both ends when using the centrifuge technique differed between species.

353 *Vulnerability curves*

354 Vulnerability curves (VCs) obtained with the bench dehydration technique were s-shaped for both
355 species, with significant embolism only occurring once a threshold water potential had been reached.
356 This threshold was more negative in *H. leucoptera* (-6.3 MPa) than in *H. dactyloides* (-3.8 MPa) (Fig.
357 2). VCs obtained with bench dehydration had the most negative P_{12} and the steepest slopes of all

Con formato: Fuente: Cursiva

1
2
3
4
5
6
7
8 358 methods (Table S2), meaning that embolism formation started at more negative Ψ_x and conductivity
9 359 was lost across a narrower range of Ψ_x compared with VCs generated by centrifugation.

11
12 360 When the centrifuge was used to induce embolism, results in the shorter-vesseled species, *H.*
13 361 *dactyloides*, were similar for the three techniques used to measure loss of conductivity, flowmeter,
14 362 Cavitron and microCT (average P_{50} with the 27 cm rotor in the static centrifuge and the Cavitron -4.8
15 363 MPa), and the CI at 95% overlapped with bench dehydration ($P_{50} = -5.0$ MPa). The VC generated with
16 364 the 14 cm rotor for *H. dactyloides* yielded slightly less negative values ($P_{50} = -4.3$ MPa; Table S2; Fig.
17 365 2). In contrast, VCs for *H. leucoptera* differed considerably depending on the method and the sample
18 366 length. Vulnerability parameters (P_{12} , P_{50} , P_{88}) obtained with the Cavitron (-5.0, -7.1 and -9.0 MPa,
19 367 respectively) matched more closely with the bench dehydration VC (-6.3, -7.4 and -8.2 MPa). For
20 368 samples spun in the static centrifuge, we found a significant effect both of the rotor size and the
21 369 segment used to measure flow (whole, spun segment or excised middle section in the 27 cm rotor) on
22 370 apparent vulnerability to embolism: segments measured across their entire length exhibited higher
23 371 vulnerability to embolism compared to the bench-dehydration VC as shown by P_{12} (-1.2 and -2.6 MPa
24 372 for 14 and 27 cm rotors, respectively) and P_{50} (-5.3 and -6.0 MPa, respectively), but seemed less
25 373 vulnerable towards the dry end of the curve (P_{88} of -14.2 and -10.4 MPa, respectively; Table S2). Both
26 374 VCs were almost linear when flow was measured across the whole segment with a shift towards more
27 375 vulnerable values with the 14 cm rotor, but became s-shaped when only the middle section of the 27
28 376 cm segment was measured (Fig. 2). Removing the segment ends resulted in a steeper slope and
29 377 significantly more negative values of P_{12} and P_{50} . The Cavitron and the middle segment techniques
30 378 yielded similar results and agreed well with the dehydration technique in P_{50} and P_{88} and with microCT
31 379 image analysis (red triangles in Fig. 2).

380 *Patterns of embolism across a centrifuged sample*

381 Within 27-cm-length centrifuged samples of *H. leucoptera*, microCT scans revealed that embolism
382 levels were consistently at their highest near the sample ends (at 12 cm from the axis of rotation)

1
2
3
4
5
6
7
8 383 when spun at equivalents of -5, -7 and -9 MPa in the static centrifuge (Fig. 3). At -5 and -7 MPa loss of
9
10 384 conductivity decreased from the basal end to the centre, contradicting theoretical expectations. This
11
12 385 trend was observed even at Ψ_x inducing less than 40% PLC based on the bench dehydration VC (Fig.
13
14 386 3). Only at -9 MPa, that is, below P_{88} on bench dehydration, did levels of embolism converge along the
15
16 387 length of the sample at 80-90%.

17 388 *Influence of open vessels in the VC of a centrifuged sample*

18
19 389 The simulations produced by the CAVITOPEN model confirmed that the shape of the VCs generated
20
21 390 by the centrifugation was largely dependent on vessel and sample lengths. As maximum vessel length
22
23 391 decreased, PLC of the whole sample decreased at a given Ψ_x , and the shape of the VC shifted from
24
25 392 exponential to sigmoidal (Fig. 4a). The same pattern was observed when the sample length increased
26
27 393 (Fig. 4b). For instance, with 14-cm-length centrifuged samples, P_{50} ranged from -0.6 MPa to -7.7 MPa
28
29 394 varying the maximum vessel length of the sample from 50 cm to 5 cm. Likewise, the P_{50} of a centrifuged
30
31 395 sample with maximum vessel length of 15 cm ranged from -2.1 MPa in the 14-cm rotor to -7.7 MPa
32
33 396 using a 40-cm rotor. Embolism of vessels open from the cut surface (Fig. S1) influenced values of PLC
34
35 397 at high negative pressures, even in short-vesseled samples, resulting in rapid loss of conductivity
36
37 398 followed by a plateau. The more open vessels and the less negative the threshold of embolism of open
38
39 399 vessels (Fig. 4c), the higher is this plateau and stronger the impact on the VC (Fig. 4). VCs can be
40
41 400 corrected if the first inflection point of the curve is considered the starting point for initial conductivity
42
43 401 (K_i), i.e. 0% loss of conductivity. This is shown in Fig. 4d with actual measurements of PLC obtained in
44
45 402 27-cm centrifuged samples of *H. leucoptera*. When the CAVITOPEN model was fit (black circles and
46
47 403 grey solid line, respectively) and we used the inflection point as starting point for K_i , the corrected
48
49 404 curve matched the reference VC obtained with bench dehydration (Fig. 4d black solid line and orange
50
51 405 dashed line, respectively). Alternatively, by fitting the model using numerical optimization we
52
53 406 estimated values of $P_{50} = -6.9$ MPa, $S_{50} = 49.7$, $L_{max} = 15.21$ and $P_{open} = -0.75$.

51 407 **Discussion**

1
2
3
4
5
6
7
8 408 We evaluated the reliability of two centrifuge based techniques commonly used to measure
9
10 409 vulnerability to embolism in angiosperm species and present a protocol that mitigates experimental
11
12 410 artefacts associated with open xylem vessels. Both the static centrifuge method and the *in-situ* flow
13
14 411 centrifuge method (Cavitron) were prone to artefactual embolism caused by open vessels, although
15
16 412 the errors were significantly greater in the static centrifuge method. In a species with maximum vessel
17
18 413 length longer or similar to the centrifuge rotor diameter, the static centrifuge significantly
19
20 414 overestimated xylem vulnerability to embolism if the whole spun segment was used to measure flow.
21
22 415 Observations with microCT indicated that artefactual embolism caused by centrifugation of samples
23
24 416 occurred in the outer most portions of samples. However, we demonstrated that artefactual
25
26 417 embolism was largely eliminated from static centrifuge if flow was measured in an excised central part
27
28 418 of the segment. This altered protocol yielded VCs similar to those obtained on the same species with
29
30 419 bench dehydration thus allowing these centrifuge techniques to accurately measure vulnerability to
31
32 420 embolism in longer vesseled species. We also present a new model (CAVITOPEN) that simulates the
33
34 421 impact of vessel draining at the cut end on the whole VC curve and showed that errors were largely
35
36 422 dependent on vessel length and rotor diameter. This model allows researchers to quantitative test
37
38 423 and avoid errors associated with the artefactual embolism. The bench dehydration technique
39
40 424 indicated that significant embolism was only initiated in both species after water potential dropped
41
42 425 below a threshold value, -3.8 MPa in *H. dactyloides* and -6.3 MPa in *H. leucoptera*. PLC then increased
43
44 426 rapidly and hydraulic conductivity was lost almost completely within a span of 1 MPa (Fig. 2). These
45
46 427 vulnerability curves have been classified as sigmoidal or s-shaped as opposed to exponential or r-
47
48 428 shaped curves, characterized by rapid conductivity losses as soon as the water potential declines
49
50 429 below zero (Cochard et al. 2013; Sperry et al. 2012). A third type of VC, intermediate between these
51
52 430 two, exhibits a linear response, and is mainly found in diffuse porous species when using
53
54 431 centrifugation to induce embolism (Cochard et al. 2013).

55
56
57
58
59
60 432 Our results showed that VCs obtained with the static centrifuge technique and the Cavitron are similar
433 to bench dehydration in a short-vesseled species, i.e. a species with no through vessels (open at both

ends) in the segment and with few vessels open from the cut surface to the middle of the segment.

All centrifuge generated VCs for *H. dactyloides* were sigmoidal and similar to bench dehydration VCs, with a slight shift towards more vulnerable values when using the 14 cm rotor (Fig. 2, Table S2) as recently found by Pengxian et al. (2018) in *Acer mono* when comparing in the static centrifuge the 14 cm and 27 cm rotors. VCs of other short vesseled angiosperms such as *Betula pendula* (Cochard et al. 2010), *Fagus sylvatica* (Aranda et al. 2014), *Populus tremuloides* (Schreiber et al. 2011) or *Acer negundo* (Christman et al. 2009) were also sigmoidal when the static centrifuge or the Cavitron were used. In contrast, the VC shape obtained for *H. leucoptera* samples differed significantly depending on methodology resulting in a shift of P_{50} of 2 MPa in samples from the same population (Fig. 2, Table S2). This dramatic change was observed previously in peach (*Prunus persica*) when the length of the centrifuged samples was varied in a Cavitron; shorter samples were more vulnerable to embolism (P_{50} shifted from -4.5 to -1 MPa) and VCs became r-shaped (Cochard et al. 2010). However, when using the static centrifuge to measure the same population, Sperry et al. (Sperry et al. 2012) found that VCs were linear and relatively insensitive to the number of open vessels with P_{50} less negative than -2 MPa using 14 cm and 27 cm samples. This difference in sensitivity to the proportion of open vessels in the centrifuged samples has led some to conclude that the original centrifuge method and rotor design are not subject to the open vessel artefact (Hacke et al. 2015; Sperry et al. 2012). However, Torres-Ruiz et al. (2017) demonstrated that if the amount of open vessels is relatively high in both rotors, 14 and 27 cm, VCs could be equally biased and would appear statistically indistinguishable.

Recent publications have addressed this controversy, showing that long-vesseled species such as grape vine, oaks, robinia or olive, with a high proportion of open vessels, produce similarly biased results with both the static centrifuge and the Cavitron when compared with reference curves generated by dehydration or non-invasive imaging (Choat et al. 2016; Choat et al. 2010; Pengxian et al. ; Torres-Ruiz et al. 2014). Li et al. (2008) and Pengxian et al. (2018) tested the two centrifuge methods head to head and found close correspondence in VCs across species with different xylem anatomy. An extended literature survey of methods to measure vulnerability to embolism showed

1
2
3
4
5
6
7
8 460 that when using the centrifuge, VCs were sigmoidal in conifers and in long vessel species exponential,
9
10 461 whereas in diffuse porous species VCs varied from sigmoidal to linear or exponential (Cochard et al.
11
12 462 2013). Our measurements and simulations made with the CAVITOPEN model explain the different
13 463 shapes of VCs and some disagreements between the static centrifuge and the Cavitron. In short-
14
15 464 vesseled angiosperms, we have shown that VCs by centrifugation agreed with each other and closely
16
17 465 matched the curves based on bench dehydration and microCT (Choat et al. 2016; Cochard et al. 2010).
18
19 466 In angiosperms with a proportion of vessels open to the middle but not the whole way through, the
20
21 467 standard protocol in the static centrifuge produces linear VCs (Sperry et al. 2012). Here the initial
22
23 468 conductivity is measured before spinning, thus if the native embolism is low, all the vessels are
24
25 469 conductive, regardless of their length. As soon as the sample is spun, the conductivity would be
26
27 470 artificially reduced relative to the native state in proportion to the amount of vessels open to centre.
28
29 471 Sample with open vessels thus become artificially vulnerable to embolism at the beginning of the VC
30
31 472 (i.e. at less negative water potentials). For *H. leucomyces*, this translated into less negative values of
32
33 473 P_{12} in all centrifuged samples compared with those measured with the bench dehydration technique
34
35 474 creating a linear response or a plateau at high water potentials. Higher differences in P_{12} were
36
37 475 observed in *H. leucomyces* than in *H. dactyloides* according with a higher proportion of vessels open to
38
39 476 centre in the former species (Fig. 1). In the Cavitron, the initial measurement was made while spinning
40
41 477 at low tension and many open to centre vessels would already be embolised in the initial
42
43 478 measurement of conductivity, resulting in a lower artefactual loss of conductivity in the subsequent
44
45 479 water potentials of the VC. This may bias the curves slightly pushing them to more negative values but
46
47 480 it did not appear to be significant effect here as the Cavitron curves for *H. leucomyces* were similar to
48
49 481 bench dehydration curves.

46 482 The simulations of PLC with the CAVITOPEN model confirmed that the impact of open vessels on the
47
48 483 VC was higher when vessels were long, samples short and when open vessels cavitated at less negative
49
50 484 pressures (Fig. 4). If the samples were much shorter than the maximum vessel length of the branch
51
52 485 (see the results in Fig. 4 for the 14 cm rotor with L_{max} 50cm), the resulting VC was exponential (r-

20

1
2
3
4
5
6
7
8 486 shaped), as observed in long-vesseled angiosperms, and shifted to more linear or s-shaped when L_{max}
9
10 487 was decreased or the sample length increased. One of the assumptions in the model is that vessels
11
12 488 open at the cut surface cavitate when they reach a threshold value; that is far less negative than intact
13
14 489 vessels whose two ends are included within the spun segment. This influences the shape the VC at
15
16 490 higher pressures creating a “bump” in the VC followed by a plateau. This effect can be corrected to
17
18 491 some extent if the first inflexion point of the VC is considered to be the 0% point for loss of
19
20 492 conductivity. In this case the initial conductivity (K_i) value is shifted to a lower value corresponding to
21
22 493 the hydraulic conductivity of the plateau (Fig. 4d). The estimated values of P_{50} and S_{50} when the
23
24 494 CAVITOPEN model was fit to actual measurements agreed quite well with those obtained with
25
26 495 reference techniques and confirmed that this model can be used to correct open vessel artefacts for
27
28 496 centrifuge based VCs. The estimated L_{max} was however significantly shorter than L_{max} measured with
29
30 497 the air injection technique. The air injection technique has shown to produce higher L_{max} than the
31
32 498 rubber injection method (Pan et al. 2015), thus our values could be overestimated. On the other hand,
33
34 499 the model assumed that vessel lengths in a sample follow the density function proposed by Cohen et
35
36 500 al. (2003) which can be sensitive to the clustering of vessel lengths (Cai and Tyree 2014). It is clear that
37
38 501 the actual distribution of vessel lengths, network topology and connectivity are crucial for the
39
40 502 sensitivity to an open vessel artefact.

503 **Origin of the open-vessel artefact**

40 504 The physical mechanisms underlying this open-vessel artefact are yet to be fully elucidated. Some
41
42 505 studies suggest that microbubbles and particles can act as nucleation sites when they flow through
43
44 506 the sample as it spins in the Cavitron, causing premature embolism (Cochard et al. 2010; Sperry et al.
45
46 507 2012; Wang et al. 2014). In the static centrifuge, bubbles might be drawn into vessels while starting
47
48 508 the spin or while mounting or dismounting the stems to measure flow (Wang et al. 2014). In both
49
50 509 centrifuge techniques bubbles in open vessels can move by buoyancy while spinning toward the region
51
52 510 of lowest pressure at the center of rotation (Rockwell et al., 2014). Draining from open vessels as a

1
2
3
4
5
6
7
8 511 consequence of artefactual embolism when the centrifuge starts spinning appears to be a common
9
10 512 phenomenon in both rotors. Our microCT images showed that after spinning in the centrifuge, most
11
12 513 of the vessels were empty near the ends even though tension ought to be zero (Cochard et al. 2005).
13 514 The use of water saturated foam pads to avoid desiccation did not prevent this (Hacke et al. 2015;
14
15 515 Tobin et al. 2013). We discarded the possibility that sample manipulation before spinning or during
16
17 516 wax embedding had triggered vessel draining because we scanned control samples that were not
18
19 517 spun. These samples showed no embolism (Fig. 3). Furthermore, patterns of embolism did not follow
20
21 518 theoretical expectations based on the distribution of tension within the spun sample. The embolism
22
23 519 levels decreased from the ends to the center in a fashion consistent with the amount of vessels open
24
25 520 to center, opposite to that expected from profile in tension and in agreement with the assumption of
26
27 521 the CAVITOPEN model than open vessels artificially cavitate when they reach a threshold pressure
28
29 522 that is much less negative than in intact vessels. This pattern was observed at water potentials
30
31 523 inducing less than 40% loss of conductivity based on the VC obtained using the middle segment of the
32
33 524 centrifuged sample (Fig. 3), even though the centre of the sample experienced the highest tensions.
34
35 525 Embolism levels converged within the sample at -9 MPa at 80-90%. These results confirm that
36
37 526 centrifugation drains open vessels and only reliably measure the vulnerability of intact xylem vessels
38
39 527 within the sample (Fig. S1). This is consistent with observations made previously by Cochard et al.
40
41 528 (2010) using the Cavitron; they reported that embolism was higher in the basal and upstream ends
42
43 529 relative to the centre of samples from species with vessels that are predominately at least half as long
44
45 530 as the spun segment. Cai et al. (2010) and Pengxian et al. (2018) also reported higher PLC values than
46
47 531 predicted by theory at both ends after spinning samples in a Cavitron. Given that our results were
48
49 532 obtained with the static centrifuge it is clear that the overestimation of vulnerability for open to centre
50
51 533 vessels occurs in both versions of the centrifuge technique.

52
53
54
55
56
57
58
59
60 534 The hydraulic continuity between vessels cut open at each end of the sample and vessels with their
61
62 535 terminal ends in this portion of the sample is probably re-established by refilling of vessels immersed
63
64 536 under water at both ends (Fig. 2 in Cochard et al. (2010)). This refilling would occur by capillarity either

1
2
3
4
5
6
7
8 537 while spinning in the Cavitron or while flow is measured gravimetrically (Fig. S2). Since the middle of
9
10 538 the centrifuged sample contains the majority of intact vessels, VCs constructed with the static
11
12 539 centrifuge technique of angiosperm species using only the central segment are more reliable and in
13
14 540 closer agreement with PLC generated by natural dehydration (Fig. 2). This modification is technically
15
16 541 easy to achieve and mitigates the open vessel artefact; however, it carries the disadvantage that
17
18 542 samples cannot be spun repeatedly to construct replicate curves for each sample and thus more plant
19
20 543 material is needed to construct each curve.

20 544 **Conclusion**

21
22
23 545 We confirmed the validity of vulnerability curves constructed with both centrifuge methods for short
24
25 546 conduit angiosperm species, those with most conduits shorter than half the length of the centrifuge
26
27 547 rotor. A new model, CAVITOPEN was developed to simulate the effect of vessel length, rotor size and
28
29 548 vulnerability of open vessels in loss of conductivity of centrifuged samples. In species with maximum
30
31 549 vessel length similar to the centrifuge rotor, we recommend constructing vulnerability curves with the
32
33 550 Cavitron or measuring flow exclusively in the central part of the spun segment when using the static
34
35 551 centrifuge. Alternatively, artefactual embolism at low xylem tensions can be corrected if the first
36
37 552 inflexion point of the VC is considered to be the starting point for K_{max} (0 % loss of conductivity) or by
38
39 553 fitting the CAVITOPEN model to the measurements to estimate P_{50} and S_{50} . When samples contained
40
41 554 a high proportion of open to centre vessels, the centrifuge technique is prone to error and
42
43 555 overestimates vulnerability to embolism. Determining the proportion of open to centre vessels or
44
45 556 performing the simple test recently proposed by Torres-Ruiz et al. (2017), which compares changes in
46
47 557 K_s before and after spinning in the centrifuge at low tensions, are highly advisable before using any of
48
49 558 the centrifuge techniques.

50
51 559 The shape of the vulnerability curves obtained with bench dehydration were always sigmoidal while
52
53 560 in centrifuged samples the shape was determined by the presence of open vessels. While previous
54
55 561 studies have demonstrated that species with the longest vessel classes (eg. lianas, ring porous trees)

1
2
3
4
5
6
7
8 562 open vessels tend to exhibit exponential curves when measured in the centrifuge. Here we showed
9
10 563 that VCs with a linear shape are symptomatic of species with intermediate vessel lengths in which a
11
12 564 higher proportion of vessels open to centre of the test segment. The occurrence of this incipient open
13
14 565 vessel artefact can be mitigated by measurement of the excised central portion of the segment.

15 566 **Acknowledgments**

16
17
18 567 This research was supported by a Marie Curie Fellowship to R.L. (FP7PEOPLE-2013-IOF-624473) and
19
20 568 an ARC Future Fellowship to B.C. (FT130101115). We thank Dr. Javier Cano, Adrián Cano, Teresa Rosas
21
22 569 and Jennifer Peters for field assistance, Dr. Iain M Young for X-ray microCT advice and comments on
23
24 570 the manuscript, Gavin McKenzie for lab support and Dr. Stephanie Stuart for her ideas and writing
25
26 571 assistance. No conflict of interests declared.

27 572

573 **References**

- 574 Alder N, Pockman W, Sperry J, Nuismer S (1997) Use of centrifugal force in the study of xylem
575 cavitation. *Journal of Experimental Botany*. 48:665-674.
- 576 Aranda I, Cano FJ, Gascó A, Cochard H, Nardini A, Mancha JA, López R, Sánchez-Gómez D (2014)
577 Variation in photosynthetic performance and hydraulic architecture across European beech
578 (*Fagus sylvatica* L.) populations supports the case for local adaptation to water stress. *Tree*
579 *physiology*. 35:34-46.
- 580 Brodersen CR, McElrone AJ, Choat B, Lee EF, Shackel KA, Matthews MA (2013) In vivo visualizations
581 of drought-induced embolism spread in *Vitis vinifera*. *Plant Physiology*. 161:1820-9.
- 582 Brodribb TJ (2017) Progressing from 'functional' to mechanistic traits. *New Phytologist*. 215:9-11.
- 583 Brodribb TJ, Cochard H (2009) Hydraulic failure defines the recovery and point of death in water-
584 stressed conifers. *Plant Physiology*. 149:575-84.
- 585 Cai J, Hacke U, Zhang S, Tyree MT (2010) What happens when stems are embolized in a centrifuge?
586 Testing the cavitron theory. *Physiologia plantarum*. 140:311-320.
- 587 Cai J, Tyree MT (2014) Measuring vessel length in vascular plants: can we divine the truth? History,
588 theory, methods, and contrasting models. *Trees*. 28:643-655.
- 589 Choat B, Badel E, Burlett R, Delzon S, Cochard H, Jansen S (2016) Noninvasive Measurement of
590 Vulnerability to Drought-Induced Embolism by X-Ray Microtomography. *Plant Physiology*.
591 170:273-82.
- 592 Choat B, Drayton WM, Brodersen C, Matthews MA, Shackel KA, Wada H, McElrone AJ (2010)
593 Measurement of vulnerability to water stress-induced cavitation in grapevine: a comparison
594 of four techniques applied to a long-veined species. *Plant, Cell & Environment*. 33:1502-12.
- 595 Choat B, Jansen S, Brodribb TJ, Cochard H, Delzon S, Bhaskar R, Bucci SJ, Feild TS, Gleason SM, Hacke
596 UG, Jacobsen AL, Lens F, Maherali H, Martinez-Vilalta J, Mayr S, Mencuccini M, Mitchell PJ,
597 Nardini A, Pittermann J, Pratt RB, Sperry JS, Westoby M, Wright IJ, Zanne AE (2012) Global
598 convergence in the vulnerability of forests to drought. *Nature*. 491:752-5.
- 599 Christman MA, Sperry JS, Adler FR (2009) Testing the 'rare pit' hypothesis for xylem cavitation
600 resistance in three species of *Acer*. *New Phytologist*. 182:664-674.
- 601 Cobb AR, Choat B, Holbrook NM (2007) Dynamics of freeze-thaw embolism in *Smilax rotundifolia*
602 (*Smilacaceae*). *American Journal of Botany*. 94:640-9.
- 603 Cochard H (2002) A technique for measuring xylem hydraulic conductance under high negative
604 pressures. *Plant, Cell & Environment*. 25:815-819.
- 605 Cochard H, Badel E, Herbette S, Delzon S, Choat B, Jansen S (2013) Methods for measuring plant
606 vulnerability to cavitation: a critical review. *Journal of Experimental Botany*. 64:4779-91.
- 607 Cochard H, Damour G, Bodet C, Tharwat I, Poirier M, Améglio T (2005) Evaluation of a new
608 centrifuge technique for rapid generation of xylem vulnerability curves. *Physiologia*
609 *Plantarum*. 124:410-418.
- 610 [Cochard H, Delzon S, Badel E \(2015\) X-ray microtomography \(micro-CT\): a reference technology for](http://mc.manuscriptcentral.com/tp)
611 [high-resolution quantification of xylem embolism in trees. *Plant, Cell & Environment*.](http://mc.manuscriptcentral.com/tp)
612 [38:201-206.](http://mc.manuscriptcentral.com/tp)
- 613 Cochard H, Ewers F, Tyree M (1994) Water relations of a tropical vine-like bamboo (*Rhipidocladum*
614 *racemiflorum*): root pressures, vulnerability to cavitation and seasonal changes in embolism.
615 *Journal of Experimental Botany*. 45:1085-1089.
- 616 Cochard H, Herbette S, Barigah T, Badel E, Ennajeh M, Vilagrosa A (2010) Does sample length
617 influence the shape of xylem embolism vulnerability curves? A test with the Cavitron
618 spinning technique. *Plant, Cell & Environment*. 33:1543-52.
- 619 Cohen S, Bennink J, Tyree M (2003) Air method measurements of apple vessel length distributions
620 with improved apparatus and theory*. *Journal of Experimental Botany*. 54:1889-1897.

- 1
2
3
4
5
6
7
- 8 621 Dalla-Salda G, Fernández ME, Sergent A-S, Rozenberg P, Badel E, Martinez-Meier A (2014) Dynamics
9 622 of cavitation in a Douglas-fir tree-ring: transition-wood, the lord of the ring? *Journal of Plant*
10 623 *Hydraulics*. 1:005.
- 11 624 Duursma R (2017) An R implementation of the CAVITOPEN model
12 625 Duursma R, Choat B (2017) fitplc - an R package to fit hydraulic vulnerability curves. 2017. 4
- 13 626 Ennajeh M, Simoes F, Khemira H, Cochard H (2011) How reliable is the double-ended pressure sleeve
14 627 technique for assessing xylem vulnerability to cavitation in woody angiosperms? *Physiologia*
15 628 *Plantarum*. 142:205-10.
- 16 629 Ewers FW, Fisher JB (1989) Variation in vessel length and diameter in stems of six tropical and
17 630 subtropical lianas. *American Journal of Botany*:1452-1459.
- 18 631 Hacke UG, Venturas MD, MacKinnon ED, Jacobsen AL, Sperry JS, Pratt RB (2015) The standard
19 632 centrifuge method accurately measures vulnerability curves of long-vesselled olive stems.
20 633 *New Phytologist*. 205:116-27.
- 21 634 Holbrook NM, Burns MJ, Field CB (1995) Negative xylem pressures in plants: a test of the balancing
22 635 pressure technique. *Science*. 270:1193-1195.
- 23 636 Jacobsen AL, Pratt RB (2012) No evidence for an open vessel effect in centrifuge-based vulnerability
24 637 curves of a long-vesselled liana (*Vitis vinifera*). *New Phytologist*. 194:982-990.
- 25 638 Jansen S, Schuldt B, Choat B (2015) Current controversies and challenges in applying plant hydraulic
26 639 techniques. *New Phytologist*. 205:961-964.
- 27 640 Li Y, Sperry JS, Taneda H, Bush SE, Hacke UG (2008) Evaluation of centrifugal methods for measuring
28 641 xylem cavitation in conifers, diffuse- and ring-porous angiosperms. *New Phytologist*.
29 642 177:558-68.
- 30 643 Nardini A, Battistuzzo M, Savi T (2013) Shoot desiccation and hydraulic failure in temperate woody
31 644 angiosperms during an extreme summer drought. *New Phytologist*. 200:322-329.
- 32 645 Nolf M, Lopez R, Peters JM, Flavel RJ, Koloadin LS, Young IM, Choat B (2017) Visualization of xylem
33 646 embolism by X-ray microtomography: a direct test against hydraulic measurements. *New*
34 647 *Phytologist*. 214:890-898.
- 35 648 Ogle K, Barber JJ, Willson C, Thompson B (2009) Hierarchical statistical modeling of xylem
36 649 vulnerability to cavitation. *New Phytologist*. 182:541-554.
- 37 650 Pan R, Geng J, Cai J, Tyree MT (2015) A comparison of two methods for measuring vessel length in
38 651 woody plants. *Plant, Cell & Environment*. 38:2519-2526.
- 39 652 Pengxian Y, Feng M, Qing L, Rui A, Jing C, Guangyuan D A comparison of two centrifuge techniques
40 653 for constructing vulnerability curves: insight into the 'open-vessel' artifact. *Physiologia*
41 654 *Plantarum*. 0
- 42 655 Pockman WT, Sperry JS, Leary JW (1995) Sustained and significant negative water pressure in xylem.
43 656 *Nature*. 378:715.
- 44 657 Rodríguez-Calcerrada J, Li M, López R, Cano FJ, Oleksyn J, Atkin OK, Pita P, Aranda I, Gil L (2017)
45 658 Drought-induced shoot dieback starts with massive root xylem embolism and variable
46 659 depletion of nonstructural carbohydrates in seedlings of two tree species. *New Phytologist*.
47 660 213:597-610.
- 48 661 Sala A, Piper F, Hoch G (2010) Physiological mechanisms of drought-induced tree mortality are far
49 662 from being resolved. *New Phytologist*. 186:274-81.
- 50 663 Schneider CA, Rasband WS, Eliceiri KW (2012) NIH Image to ImageJ: 25 years of image analysis.
51 664 *Nature methods*. 9:671-675.
- 52 665 Schreiber SG, Hacke UG, Hamann A, Thomas BR (2011) Genetic variation of hydraulic and wood
53 666 anatomical traits in hybrid poplar and trembling aspen. *New Phytologist*. 190:150-160.
- 54 667 Sperry JS (1985) Xylem embolism in the palm *Rhapis excelsa*. *IAWA Journal*. 6:283-292.
- 55 668 Sperry JS, Christman MA, Torres-Ruiz JM, Taneda H, Smith DD (2012) Vulnerability curves by
56 669 centrifugation: is there an open vessel artefact, and are 'r' shaped curves necessarily invalid?
57 670 *Plant, Cell & Environment*. 35:601-10.

- 1
2
3
4
5
6
7
8 671 Sperry JS, Tyree MT (1988) Mechanism of water stress-induced xylem embolism. *Plant Physiology*.
9 672 88:581-7.
10 673 Tobin MF, Pratt RB, Jacobsen AL, De Guzman ME (2013) Xylem vulnerability to cavitation can be
11 674 accurately characterised in species with long vessels using a centrifuge method. *Plant*
12 675 *Biology*. 15:496-504.
13 676 Torres-Ruiz JM, Cochard H, Mayr S, Beikircher B, Diaz-Espejo A, Rodriguez-Dominguez CM, Badel E,
14 677 Fernandez JE (2014) Vulnerability to cavitation in *Olea europaea* current-year shoots: further
15 678 evidence of an open-vessel artifact associated with centrifuge and air-injection techniques.
16 679 *Physiologia Plantarum*. 152:465-74.
17 680 Torres-Ruiz JM, Cochard H, Mencuccini M, Delzon S, Badel E (2016) Direct observation and modelling
18 681 of embolism spread between xylem conduits: a case study in Scots pine. *Plant, Cell &*
19 682 *Environment*. 39:2774-2785.
20 683 Torres-Ruiz JM, Jansen S, Choat B, McElrone AJ, Cochard H, Brodribb TJ, Badel E, Burrett R, Bouche
21 684 PS, Brodersen CR (2015) Direct X-ray microtomography observation confirms the induction
22 685 of embolism upon xylem cutting under tension. *Plant Physiology*. 167:40-43.
23 686 Torres-Ruiz JM, Cochard H, Choat B, Jansen S, López R, Tomášková I, Padilla-Díaz CM, Badel E, Burrett
24 687 R, King A (2017) Xylem resistance to embolism: presenting a simple diagnostic test for the
25 688 open vessel artefact. *New Phytologist*. 215:489-499.
26 689 Tyree MT, Dixon MA (1986) Water stress induced cavitation and embolism in some woody plants.
27 690 *Physiologia Plantarum*. 66:397-405.
28 691 Tyree MT, Sperry JS (1988) Do woody plants operate near the point of catastrophic xylem
29 692 dysfunction caused by dynamic water stress? : answers from a model. *Plant Physiology*.
30 693 88:574-80.
31 694 Tyree MT, Zimmermann MH (2002) Hydraulic architecture of whole plants and plant performance
32 695 Xylem structure and the ascent of sap. Springer, pp 175-214.
33 696 Urli M, Porte AJ, Cochard H, Guengant Y, Burrett R, Delzon S (2013) Xylem embolism threshold for
34 697 catastrophic hydraulic failure in angiosperm trees. *Tree Physiology*. 33:672-83.
35 698 Venturas MD, MacKinnon ED, Dario HL, Jacobsen AL, Pratt RB, Davis SD (2016) Chaparral shrub
36 699 hydraulic traits, size, and life history types relate to species mortality during California's
37 700 historic drought of 2014. *PLoS one*. 11:e0159145.
38 701 Wang R, Zhang L, Zhang S, Cai J, Tyree MT (2014) Water relations of *Robinia pseudoacacia* L.: do
39 702 vessels cavitate and refill diurnally or are R-shaped curves invalid in *Robinia*? *Plant, cell &*
40 703 *environment*. 37:2667-2678.
41 704 Wheeler JK, Huggett BA, Tofte AN, Rockwell FE, Holbrook NM (2013) Cutting xylem under tension or
42 705 supersaturated with gas can generate PLC and the appearance of rapid recovery from
43 706 embolism. *Plant, Cell & Environment*. 36:1938-1949.

707

708

709 **Figure legends**

710 **Figure 1.** Distribution of PLC in air-injected branches of *H. dactyloides* (black circles) and *H.*
 711 *leucoptera* (open circles) at different positions from the injected end. Vertical bars represent the
 712 standard error. Dashed lines indicate the two sample lengths used for the centrifuge methods, 14 cm
 713 and 27 cm and dot lines indicate their respective half sample length.

714 **Figure 2.** Xylem vulnerability to embolism curves and 95% confidence intervals (grey shaded areas)
 715 of *Hakea dactyloides* (left panels) and *Hakea leucoptera* (right panels) obtained with two methods to
 716 induce cavitation in the xylem, bench dehydration and centrifuge force and three methods to
 717 measure the loss of conductivity, flowmeter (close circles), in situ flow method (open circles) and X-
 718 ray microCT visualisation (red triangles). Vertical solid lines indicate P_{50} and vertical dashed lines
 719 indicate the 95% confidence interval for P_{50} . [Horizontal dashed lines indicated native xylem](#)
 720 [embolism measured in the field.](#) Two rotor sizes, 14 cm and 27 cm, were used in the static
 721 centrifuge, and water flow in the whole segment or only in the central part was measured (see
 722 methods for details).

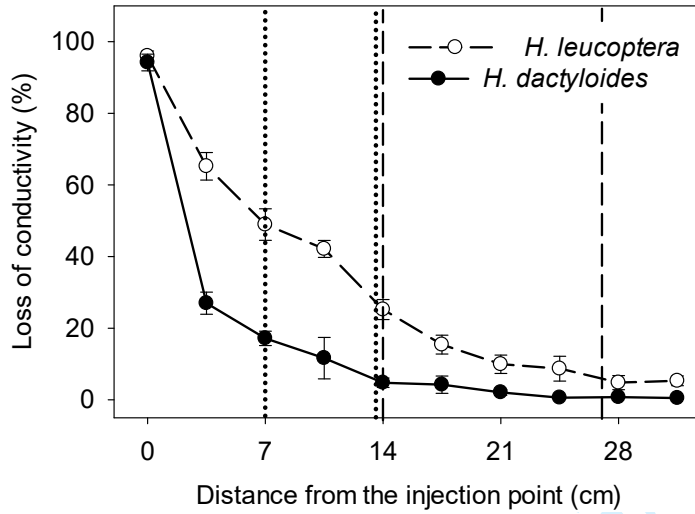
723 **Figure 3.** Transverse slices from X-ray microtomography (X-ray micro-CT) scans of branches of *Hakea*
 724 *leucoptera* (maximum vessel length = 25 ± 5 cm) scanned at three positions before spinning (left
 725 column) and after spinning in the centrifuge at 5, 7 and 9 MPa. Embolized vessels appear as black
 726 and water-filled conduits appear as grey. The estimated percent loss of conductivity (PLC) is shown
 727 in each picture. Scale bar, 1 mm.

728 **Figure 4.** Simulations with the CAVITOPEN model of the effect of threshold of embolism formation
 729 (MPa) of cut open vessels (A), maximum vessel length (cm) (B), and rotor size (cm) (C) on xylem
 730 vulnerability to embolism curves generated with centrifugation. In red, vulnerability curve of close
 731 vessels at both ends. (D) The CAVITOPEN model was fit to measurements in *H. leucoptera* using
 732 numerical optimization to estimate all four parameters: water potential at 50% loss of conductivity

1
2
3
4
5
6
7
8 733 (P_{50}), slope of the vulnerability curve (S_{50}), maximum vessel length (L_{max}) and threshold of embolism
9 734 formation of cut open vessels (P_{open}). Circles represent the values obtained in our study with the static
10 735 centrifuge, 27 cm rotor in *H. leucoptera* when flow was measured in the whole segment (see Methods
11 736 for details); grey solid line is the fitted curve with the CAVITOPEN model; black solid line represent the
12 737 curve after correction and orange dashed line is the reference curve obtained with bench dehydration
13 738 for the species.
14
15
16
17
18
19 739

For Peer Review

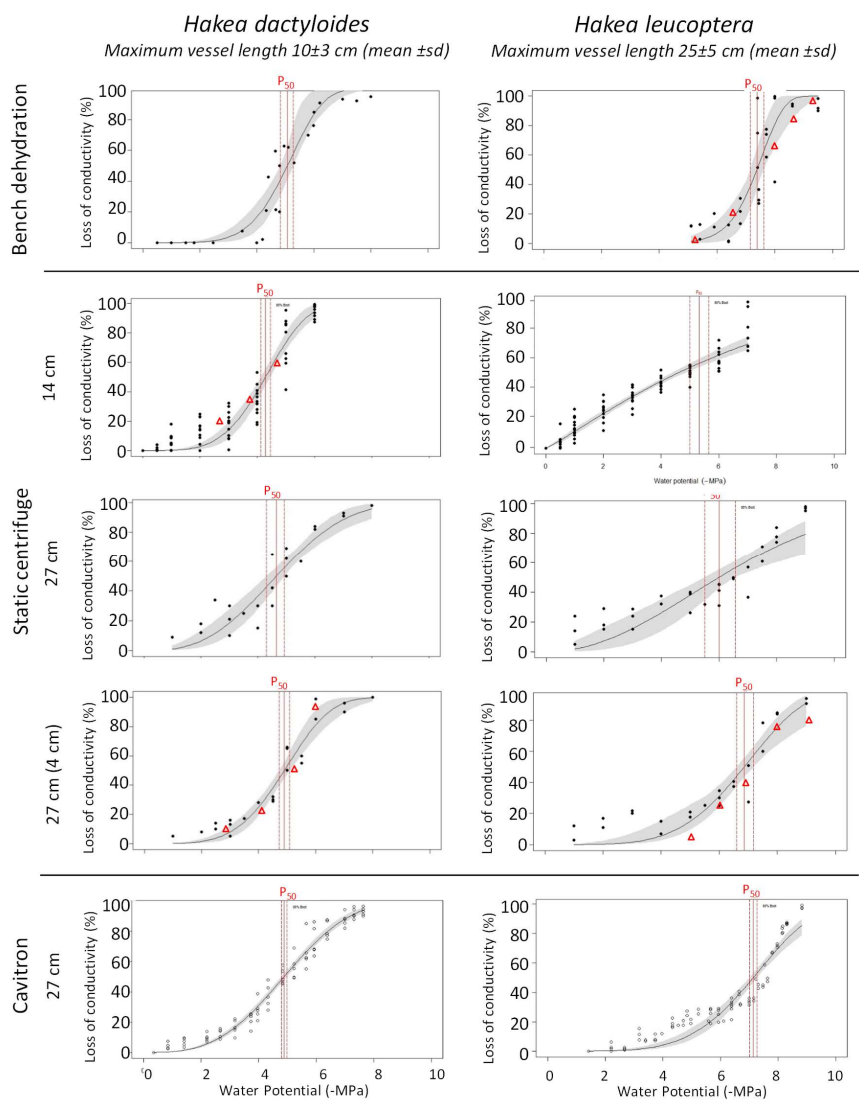
740 Figures



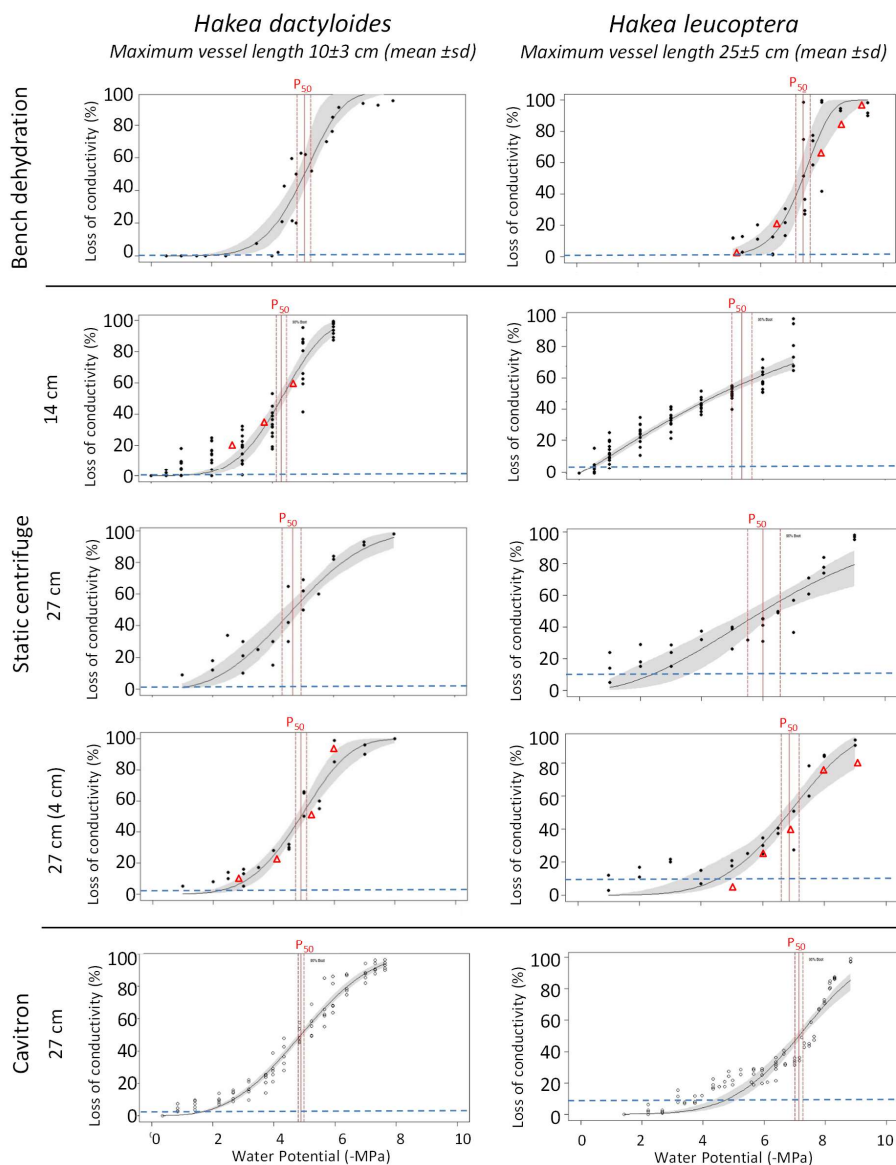
741

742 **Figure 1.** Distribution of PLC in air-injected branches of *H. dactyloides* (black circles) and *H.*
 743 *leuoptera* (open circles) at different positions from the injected end. Vertical bars represent the
 744 standard error. Dashed lines indicate the two sample lengths used for the centrifuge methods, 14 cm
 745 and 27 cm and dot lines indicate their respective half sample length.

746



747

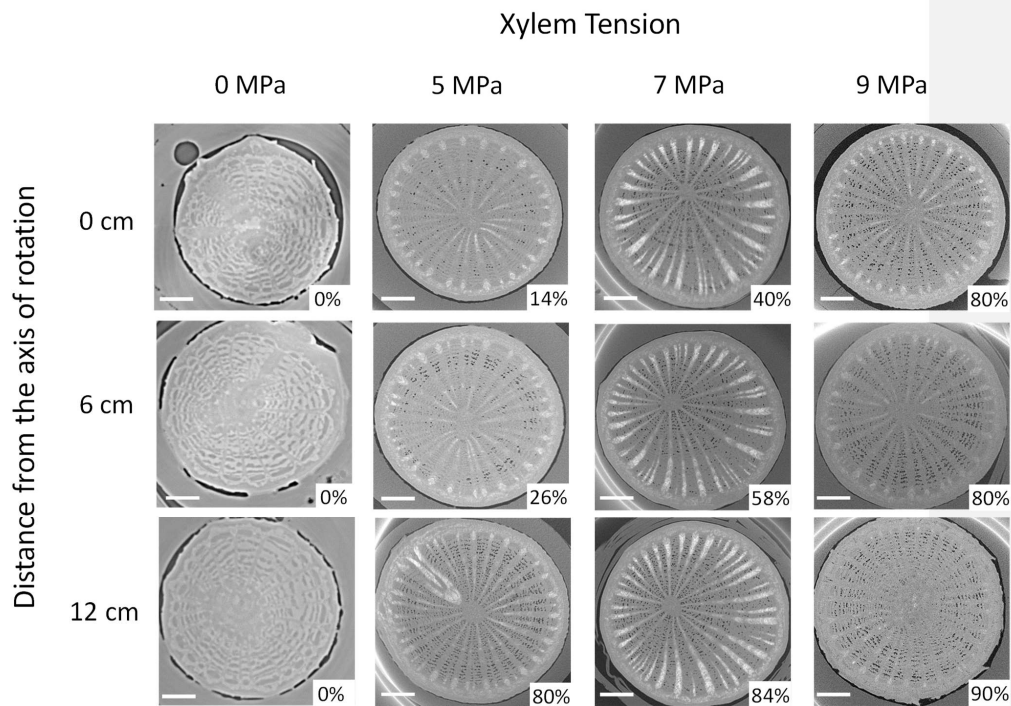


748

749 **Figure 2.** Xylem vulnerability to embolism curves and 95% confidence intervals (grey shaded areas)
 750 of *Hakea dactyloides* (left panels) and *Hakea leucoptera* (right panels) obtained with two methods to
 751 induce cavitation in the xylem, bench dehydration and centrifuge force and three methods to
 752 measure the loss of conductivity, flowmeter (close circles), in situ flow method (open circles) and
 753 X-ray microCT visualisation (red triangles). Vertical solid lines indicate P_{50} and vertical dashed lines
 754 indicate the 95% confidence interval for P_{50} . Two rotor sizes, 14 cm and 27 cm, were used in the

32

755 static centrifuge, and water flow in the whole segment or only in the central part was measured (see
 756 methods for details).



757
 758 **Figure 3.** Transverse slices from X-ray microtomography (X-ray micro-CT) scans of branches of *Hakea*
 759 *leucoptera* (maximum vessel length = 25 ± 5 cm) scanned at three positions before spinning (left
 760 column) and after spinning in the centrifuge at 5, 7 and 9 MPa. Embolized vessels appear as black
 761 and water-filled conduits appear as grey. The estimated percent loss of conductivity (PLC) is shown
 762 in each picture. Scale bar, 1 mm.

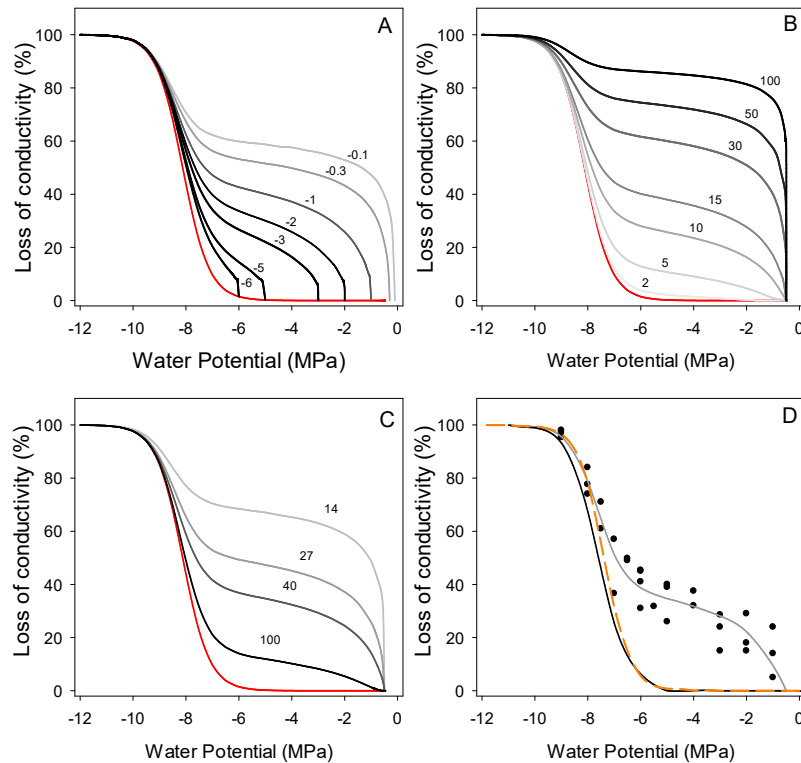


Figure 4. Simulations with the CAVITOPEN model of the effect of threshold of embolism formation (MPa) of cut open vessels (A), maximum vessel length (cm) (B), and rotor size (cm) (C) on xylem vulnerability to embolism curves generated with centrifugation. In red, vulnerability curve of close vessels at both ends. (D) The CAVITOPEN model was fit to measurements in *H. leucoptera* using numerical optimization to estimate all four parameters: water potential at 50% loss of conductivity (P_{50}), slope of the vulnerability curve (S_{50}), maximum vessel length (L_{max}) and threshold of embolism formation of cut open vessels (P_{open}). Circles represent the values obtained in our study with the static centrifuge, 27 cm rotor in *H. leucoptera* when flow was measured in the whole segment (see Methods for details); grey solid line is the fitted curve with the CAVITOPEN model; black solid line represent the curve after correction and orange dashed line is the reference curve obtained with bench dehydration for the species.

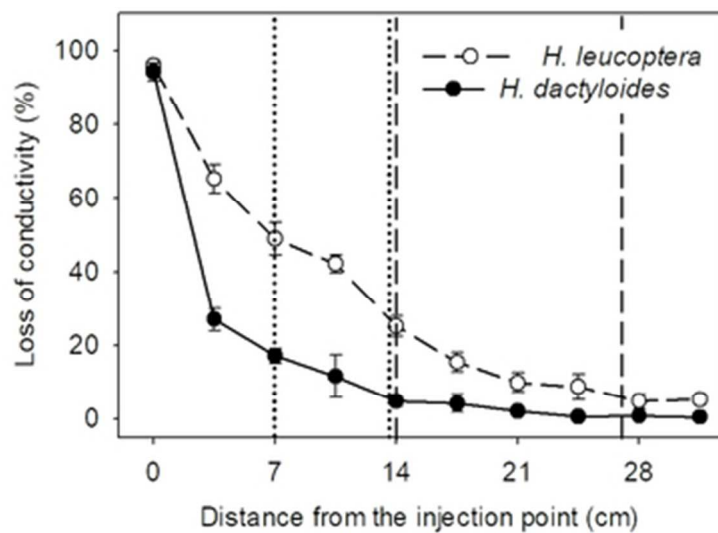


Figure 1. Distribution of PLC in air-injected branches of *H. dactyloides* (black circles) and *H. leucoptera* (open circles) at different positions from the injected end. Vertical bars represent the standard error. Dashed lines indicate the two sample lengths used for the centrifuge methods, 14 cm and 27 cm and dot lines indicate their respective half sample length.

42x32mm (300 x 300 DPI)

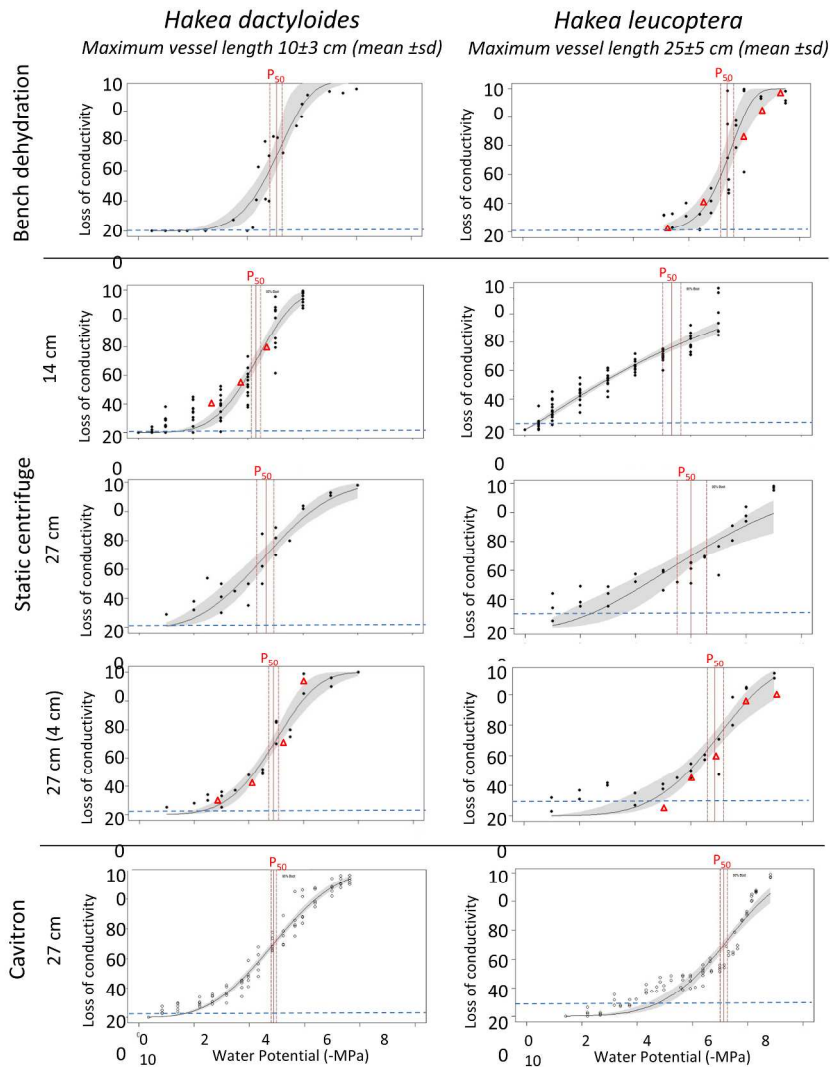


Figure 2. Xylem vulnerability to embolism curves and 95% confidence intervals (grey shaded areas) of *Hakea dactyloides* (left panels) and *Hakea leucoptera* (right panels) obtained with two methods to induce cavitation in the xylem, bench dehydration and centrifuge force and three methods to measure the loss of conductivity, flowmeter (close circles), in situ flow method (open circles) and X-ray microCT visualisation (red triangles). Vertical solid lines indicate P50 and vertical dashed lines indicate the 95% confidence interval for P50. Horizontal dashed lines indicated native xylem embolism measured in the field. Two rotor sizes, 14 cm and 27 cm, were used in the static centrifuge, and water flow in the whole segment or only in the central part was measured (see methods for details).

254x338mm (300 x 300 DPI)

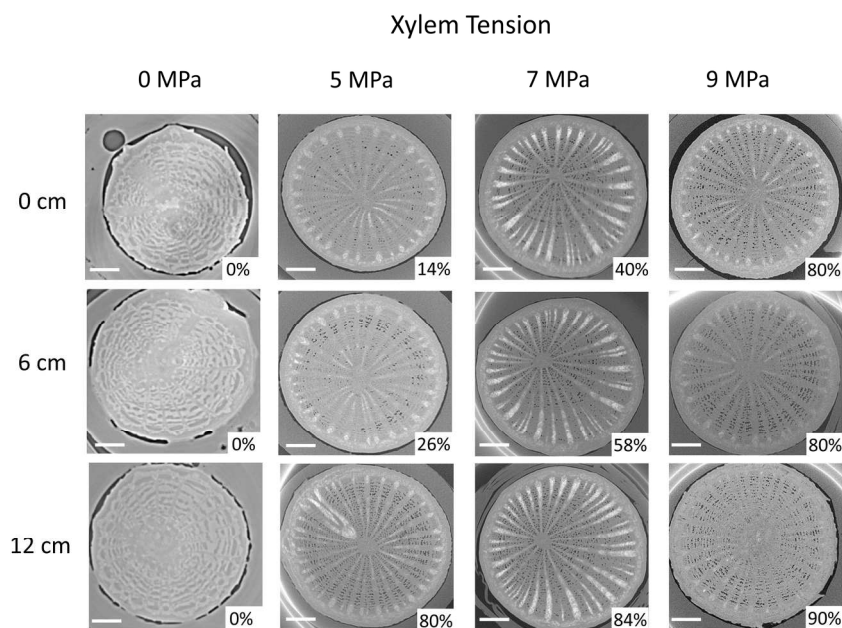


Figure 3. Transverse slices from X-ray microtomography (X-ray micro-CT) scans of branches of *Hakea leucoptera* (maximum vessel length = 25 ± 5 cm) scanned at three positions before spinning (left column) and after spinning in the centrifuge at 5, 7 and 9 MPa. Embolized vessels appear as black and water-filled conduits appear as grey. The estimated percent loss of conductivity (PLC) is shown in each picture. Scale bar, 1 mm.

190x142mm (300 x 300 DPI)

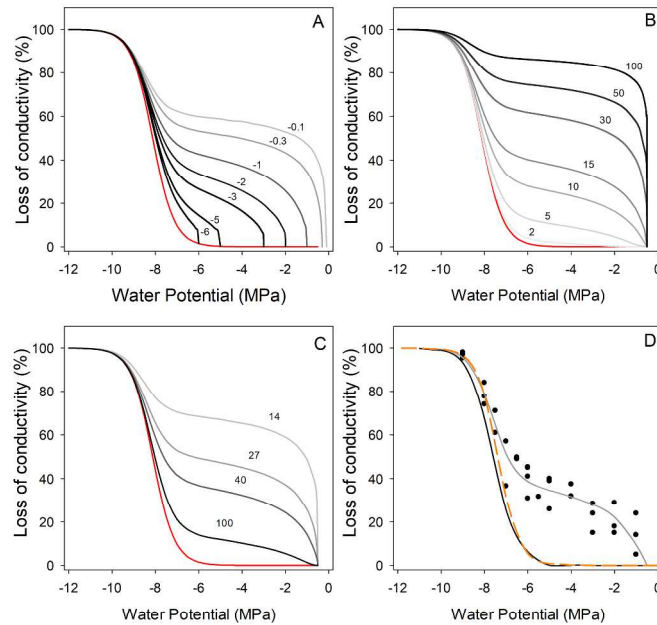


Figure 4. Simulations with the CAVITOPEN model of the effect of threshold of embolism formation (MPa) of cut open vessels (A), maximum vessel length (cm) (B), and rotor size (cm) (C) on xylem vulnerability to embolism curves generated with centrifugation. In red, vulnerability curve of close vessels at both ends. (D) The CAVITOPEN model was fit to measurements in *H. leucoptera* using numerical optimization to estimate all four parameters: water potential at 50% loss of conductivity (P_{50}), slope of the vulnerability curve (S_{50}), maximum vessel length (L_{max}) and threshold of embolism formation of cut open vessels (P_{open}). Circles represent the values obtained in our study with the static centrifuge, 27 cm rotor in *H. leucoptera* when flow was measured in the whole segment (see Methods for details); grey solid line is the fitted curve with the CAVITOPEN model; black solid line represent the curve after correction and orange dashed line is the reference curve obtained with bench dehydration for the species.

254x338mm (300 x 300 DPI)

1
2
3
4
5
6
7
8
9
10
11
12
13
14
15
16
17
18
19
20
21
22
23
24
25
26
27
28
29
30
31
32
33
34
35
36
37
38
39
40
41
42
43
44
45
46
47
48
49
50
51
52
53
54
55
56
57
58
59
60

For Peer Review